STRUCTURAL AND MAGNETIC STUDIES OF Al-BASE RARE EARTH ALLOYS

by

J. Roland Pitts

Submitted to the Faculty of the Oregon Graduate Center in partial fulfillment of the requirements for the degree of Master of Science.

Oregon Graduate Center

1972

This Master's Thesis has been examined by the following committee of the Oregon Graduate Center:

Richard A. Elliott
Assistant Professor

Hans Oesterreicher
Assistant Professor

G. J. Throop
Assistant Professor

FOREWORD

The work presented in this paper is a part of a continuing program of research directed by Professor Hans Oesterreicher. The studies involve basic research into the structural and magnetic properties of rare earth – transition metal compounds.

This paper is submitted in partial fulfillment of the requirements for the Master of Science in Physics degree at the Oregon Graduate Center. The work was performed during the period from 15 June 1970 to 20 January 1972. Acknowledgement is made to the Oregon Graduate Center for a fellowship stipend, a tuition scholarship, and for the facilities and materials with which I carried out the experimental work.

I wish to express my gratitude to Professor Oesterreicher, my thesis advisor and chairman of my Ad Hoc Committee, for his guidance throughout the program. Also, I wish to thank my other committee members, Professor G. J. Throop and Professor R. Elliott, for their assistance in the academic portion of my work. In addition, I express my appreciation for the assistance rendered by members of the technical staff of the Oregon Graduate Center in various phases of my work.

Last but not least I wish to thank the United States Selective Service System for their relentless attack upon my mental and physical well-being throughout the course of my study and work.

TABLE OF CONTENTS

I. INTRODUCTION

The present work investigates structural and low temperature magnetic properties of pseudobinaries on aluminum base of two heavy rare earth metals where Al is substituted by Co and Fe. The interest in this particular study arose mainly from the following academic and applied considerations.

While the structural and magnetic behavior of the pure rare earth metals entails a considerably complex behavior which is only partly understood so far, the rare earths in a matrix of more or less electron rich partners, although somewhat less bizarre in behavior, can be studied with greater freedom as to parameters of size and electron concentration per atom (e.c.) for instance. Particularly the e.c. seems to a great extent to be responsible for systematic changes in crystal structure and the architecture of magnetic moment alignment. Recent studies on similar materials, moreover, have shown quite a complex situation concerning the magnetization process pointing at the presence of strong anisotropies as a result of crystal field effects, partial magnetic disorder and unusual domain wall effects. This study was carried out to contribute to an understanding of the complex interplay between these influences.

From an applied point of view some of our specimens were expected to show extraordinary high coercive forces which make them interesting for permanent magnet materials. The development since 1967 of superior rare earth cobalt permanent magnets, particularly on $SmCo_5$ basis, has

concentrated on the light rare earth materials because of their higher magnetizations. This is due to the experimental rule of antiparallel spin alignment between rare earth and transition metal which results either in complete ferromagnetism or ferrimagnetism between rare earth and transition metal moment according to the different summation of orbital and spin contributions for heavy and light rare earths. (L + S and L - S coupling respectively). Since there is no theoretical justification for the antiparallel coupling mode to be exclusive, it was of interest to study the possibility of breaking this coupling scheme on addition of an electron rich partner. This should result in even higher saturation moments (the highest possible) for representatives of heavy rare earths. A parallel study of alloys on light rare earth basis is also under way in this laboratory.

II. LITERATURE REVIEW

Intermetallics between Al, rare earth, and transition metals harbor a rich potential for a variety of intermediate phases and solid state properties. Nevitt,[1] for example, has pointed out the general expectations of phase stability in these and related systems. The two most prominent factors for the stabilization of an intermediate phase are summarized in the Hume-Rothery rules as the size and the free electron concentration per atom.

The most abundant structure type in rare earth alloys is the Laves phase family which forms at the composition AB_2. Elliott and Rostoker[2] and Dwight[3] have characterized the Laves phases mainly as electron compounds; that is, their occurrence is dependent on the number of delocalized electrons per atom. If the valence electron concentration is near the border of a band of stability, more complex stacking variations and stacking fault structures can be observed. Oesterreicher and Wallace[4] have explained the phase boundaries of Laves phases RCo_2-RAl_2 in terms of Fermi surface - Brillouin zone interactions.

At transition metal rich compositions, rare earths crystallize under a variety of structural principles, the structures being considered as derivatives of the Laves phases.[5] RT_3,[6] R_2T_7,[7] R_6T_{23},[8] RT_5,[9] R_2T_{17},[10] (T ~ transition metal) are commonly encountered structural types, all of which, with the exception of R_6T_{23}, have symmetries lower than cubic. Even more complex variations and transitions from one type to another have been reported in the analogous Ni system, with changes in composition and heat treatment.[11] RAl_3 and RAl_4[12] are known aluminides on rare earth basis. The interest in

Al substitutions for T is that this substitution holds promise for a variety of new ternary phases as a result of different layer stacking, size effects, and the influence of a rising electron concentration per atom (e.c.). New phases of this sort can be of particular interest magnetically.

The origin of magnetism in rare earth metals arises from unfilled 4f shells which are highly localized and shielded by conduction electrons. Embedded in the crystal this 4f configuration is subject to the crystalline field, spin orbit, and exchange interaction. Although rare earth intermetallics, with the exception of Sm and Eu compounds, exhibit generally the free tri-positive ion value in the paramagnetic and in the ordered state, there are also cases where this moment falls short of the expected theoretical value due to crystal field effects. Farrell and Wallace[13] for instance have shown that Laves phases RCo_2 exhibit the full moment while RNi_2 compounds have a partly quenched magnetic moment in the magnetically ordered state. Bleany[14] has tried to explain the low moments in RNi_2 compounds in terms of Stark splitting comparable in magnitude to the exchange interaction.

The crystal field splitting is difficult to determine quantitatively in metals since the high metallic absorption precludes optical measurements and electron spin resonance studies yield only small intensities and require single crystals. The first exact evaluation of crystal field parameters in such intermetallics may have been established by Purwins[15,16] via susceptibility and Mossbauer measurements on single crystals of $ErAl_2$. This,

however, is still somewhat controversial since neutron diffraction[17-19] and Mossbauer spectroscopy[20] show values close to the free tripositive ion value. Oesterreicher et al.[4] have found that on substitution of Al by Co in $ErAl_2$ the ordered rare earth moment is drastically decreasing toward the phase boundary. Neutron diffraction[19] on such "low moment compounds," however, has shown that this "lost" magnetic moment is "found" again in the disorder background scattering, which seems to preclude a major effect of the crystal field ~~but rather~~ and suggests a peculiar state between order and disorder in these materials. (Co here does not exhibit a magnetic moment beyond 30 mole% $ErAl_2$). A similar situation has also been found for the analogous Tb alloys[21,22]. The situation is complicated by peculiar stepwise increases of magnetization with field at cryogenic temperatures and peaking magnetizations with temperature in low fields. Further, it is found that the magnetization is not saturated but still increasing beyond 47 kOe. It has been proposed that this behavior is due either to disordered antiferromagnetic components or else is connected with anisotropy or thin domain walls. The latter has recently been found in canted magnetic structures like Dy_3Al_2[23].

Due to the limited spatial extent of the 4f electrons, magnetic order in rare earth metals and alloys is thought to arise from an indirect exchange mechanism. The most widely accepted model is that of Rudermann-Kittel[24]-Kasuya[25]- and Yoshida[26], in which a magnetic polarization of s-d conduction electrons brings about a long range f-f interaction. For simple cubic compounds Mattis[27] et al. have shown that the type of magnetic order is a

function of the free electron concentration due to a polarization of conduction electrons. Freeman et al.[28] found the valence electron polarization to be an oscillating and decaying function with pronounced maxima and minima not necessarily at the magnetic origin. In alloys of high transition metal concentration, the dominant exchange is one between the transition metals. (For details of this exchange see reference 5.)

In the present work we have concentrated particularly on a study of the dependence of the spontaneous increases in magnetization with field on powder size, the repeatability of the first effect, and the effects of different heat treatments. The relation of the presumed high anisotropy and the concommitant lower saturation moments to either the rising e.c. or to the increase in disorder in crystallographic sites was investigated by a computer study of the line intensities in Debye-Scherrer diagrams.

Of special interest was the coupling scheme and the magnitude of the remanences, particularly of materials with high transition metal concentration. Outstanding permanent magnet properties have been found with light rare earths and Co (especially on the $SmCo_5$ basis). We have been interested in a possible reversal of the coupling scheme between transition metal and rare earth spin orbital moments. It was hoped that this might be brought about by variations in the crystal structure and by an increase in the density of the e.c. (the medium affecting magnetic exchange).

III. EXPERIMENTAL

The materials used for this study were prepared by induction melting in quartz crucibles under a flow of argon. Tb and Dy came from Michigan Chemical Corporation and were 99.9% pure with respect to other rare earths and better than 99.5% total purity. Fe, Co, and Al had purities of better than 99.999% and came from American Scientific Chemical of Portland. After melting one part of the material was annealed in an evacuated quartz ampule for about 200 hours at 1000°C. The specimens were powdered under mineral oil, which was removed by washing with CCl_4. Debye-Scherrer diagrams were taken with V-filtered Cr radiation which was calibrated by means of NaCl. Phase boundaries were located by the appearance of lines characteristic of a new phase, and more accurately, by breaks in the lattice parameter - composition curves.

Magnetic studies were carried out on a commercial Foner magnetometer, which was calibrated with Ni. Precise measurements at fixed temperatures were obtained by means of an electronically regulated temperature controller using a calibrated Ge crystal an Cu-constantan thermocouples at the sample site. The sample holders were fabricated from nylon. ~~Approximate~~ saturation moments were extrapolated from plots of the magnetic moment versus reciprocal applied field.

IV. RESULTS AND DISCUSSION

A. Studies on $DyFe_2$-$DyAl_2$ and $DyCo_2$-$DyAl_2$

Introduction: - The constitution of both systems have not been previously described in the literature. The binary phases, however, are well known C15 Laves phases (see Nevitts compilation). Ternary C14 materials DyFeAl and DyCoAl have been described by Wemick et al.[33]

Only the binaries have so far been described magnetically[34,35].

RESULTS

Lattice parameters and crystal types are summarized in Table 1. C15 ($MgCu_2$ type) $DyFe_2$ is stable to a composition $Dy_{0.333}Fe_{0.452}Al_{.215}$. A C14 ($MgZn_2$ type) phase extends from $Dy_{0.333}Fe_{0.432}Al_{.35}$ to $Dy_{.333}Fe_{.292}Al_{.375}$ and a C15 type reaches from $Dy_{0.333}Fe_{0.205}Al_{0.415}$ to $DyAl_2$. A similar situation pertains in $DyCo_2$- $DyAl_2$ but here the exact phase boundaries at Co rich concentrations were not determined. The C14 type extends to $Dy_{.333}Co_{.197}Al_{.47}$ while the C15 type is stable from $Dy_{.333}Co_{.177}Al_{.490}$ on.

The distribution of transition metal (T) and Al has to be a statistical one on 16f sites in both $MgCu_2$ type phases, assuming the rare earth solely to occupy 8h sites, but ordering can in principle occur in the C14 type on 6h and 2a sites between T and Al. Table 2 shows a comparison of calculated and observed intensities for different ordering schemes at three compositions within C14 $DyFe_xAl_{1-x}$. Intensities were calculated according to the formula $I = A.F.^2 M.LP$ in which A, F, M and LP represent a scaling factor, the structure factor, the multiplicity and the Lorentz polarization factor, respectively. The free parameters were taken in analogy of the original work of Friauf on $MgZn_2$. (Beware of an error in Pearson's handbook of lattice spacings and structures of metals). The calculations suggest ordering tendencies only for the relatively transition metal rich and poor compound. $Dy_{.333}Fe_{.417}Al_{.25}$ shows some deviations from a completely statistical occupancy (ordering 3) in the direction of a preferential occupancy of the 2a site with Fe (ordering 1). (Both melted and melted and annealed specimens

Table 1. Structures and Lattice Parameters of $DyFe_2$-$DyAl_2$ and $DyCo_2$-$DyAl_2$

Composition $Dy_{.333}Fe_{.667-x}Al_x$		Structure	a_o(Å)	c_o(Å)	co/ao	Volume	Volume/ Atom
x =	.00	C15	7.324 (7.325)[1]			392.867	16.369
	.05	C15	7.348			396.741	16.531
	.10	C15	7.400			405.224	16.884
	.15	C15	7.418			408.188	17.008
	.20	C15	7.474			417.503	17.396
	.225	C15	7.479			418.341	17.432
		C14	5.312	8.643	1.627	211.226	17.602
	.25	C14	5.326	8.661	1.626	212.760	17.730
	.30	C14	5.348	8.695	1.626	215.343	17.945
	.333[2]	C14	5.376	8.713	1.621	218.076	18.173
	.35	C14	5.392	8.711	1.616	219.354	18.280
	.40	C14	5.405	8.703	1.610	220.158	18.347
		C15	7.655			448.576	18.691
	.45	C15	7.685			453.870	18.911
	.50	C15	7.709			458.136	19.089
	.55	C15	7.767			468.554	19.523
	.60	C15	7.803			475.100	19.796
	.65	C15	7.823			478.762	19.948
	.667	C15	7.835 (7.840)[1]			480.97	20.040

Composition
$Dy_{.333}(Fe,Co)_{.667-x}Al_x$

Composition	Structure	a_o	c_o	c_o/a_o	Volume	Volume/ Atom
x = .00	C15	7.187[1)]			371.23	15.47
.333[3)]	C14	5.342	8.497	1.591	209.96	17.497
.417	C14	5.403	8.565	1.585	216.536	18.044
.467	C14	5.430	8.597	1.583	219.525	18.29
	C15	7.697			456.00	19.00
.492	C15	7.701			456.72	19.03
.567	C15	7.755			466.32	19.43
.667	C15	7.835			480.97	20.040

(1) Figures taken from M.V. Nevitts compilation in P.A. Beck, ed. Electronic Structure and Alloy Chemistry of Transition Elements, Wiley, 1963.

(2) Figures taken from H. Oesterreicher, J.Less Comm. Metals, 25, 341 (1971).

(3) Figures taken from H. Oesterreicher, J. Less Comm. Metals, 25, 228 (1971).

Table 2a. Powder X-ray Diffraction Diagram of $Dy_{.333}Fe_{.417}Al_{.25}$

Material: Induction Melted and annealed (250 hrs at 1000°C)

Radiation: CrKα

Structural Data: $MgZn_2$ Type, hexagonal a=5.341Å c=8.661Å

Space Group: No. 194, D_{6h}^4- $P6_3/mmc$

Atomic Positions:

4f	1/3, 2/3, z (z = 1/16)
2a	0, 0, 0
6h	x, 2x, 1/4 (x = 5/6)

Calculated Ordering Schemes

	Ordering 1	Ordering 2	Ordering 3 (stat.)
4f	100% Dy	100% Dy	100% Dy
2a	100% Fe	100% Al	63% Fe, 37% Al
6h	50% Fe, 50% Al	83% Fe, 17% Al	63% Fe, 37% Al

h	k	ℓ	$\theta_{calc.}$	$\theta_{obs.}$	$d_{calc.}$	Relative Intensity $I_{obs.}$	I_{calc} Ord. 1	I_{calc} Ord. 2	I_{calc} Ord.3(stat)
1	0	0	14.34	14.4	4.62544	2.0	188.8	326.1	236.9
0	0	2	15.34	15.4	4.33050	1.7	216.8	68.3	150.3
1	0	1	16.30	16.35	4.08005	1.7	218.7	153.1	192.3
1	0	2	21.24	21.25	3.16125	1.7	137.1	288.8	188.4
1	1	0	25.40	25.63	2.67050	8	848.7	612.3	753.9
1	0	3	27.89	27.98	2.44909	9	1000.0	1000.0	1000.0
2	0	0	29.69	29.75	2.31272	2	137.1	210.4	163.2
1	1	2	30.26	30.35	2.27304	10	987.9	816.8	920.7
2	0	1	30.84	31.06	2.23443	4	408.2	484.8	436.7
0	0	4	31.94	31.95	2.16525	0.5	45.0	42.4	44.0
2	0	2	34.16		2.04002		.3	.5	.0
1	0	4	35.74	35.75	1.96102	0.3	35.7	15.4	26.9
2	0	3	39.39	39.40	1.80497	1	102.8	66.1	87.9
2	1	0	40.93	40.93	1.74825	0.5	29.6	46.9	35.7
2	1	1	41.94	41.94	1.71368	0.5	40.8	29.7	36.4
1	1	4	42.93		1.68187		.8	2.2	.0
1	0	5	44.92	44.84	1.62217	2.5	179.0	155.9	170.0
2	1	2	44.96		1.62213		44.2	86.0	58.5
2	0	4	46.44		1.58062		.1	8.3	1.8
3	0	0	47.98	48.05	1.54181	2	190.4	140.4	170.4
3	0	1	48.99		1.51794		.0	.0	.0
2	1	3	49.99	50.00	1.49543	5.5	563.3	561.0	562.4
3	0	2	52.06	52.10	1.45249	3.5	338.8	282.4	316.7
0	0	6	52.52		1.44350		46.9	63.0	52.7
2	0	5	55.71	55.71	1.38643	4.5	432.9	465.0	445.0
1	0	6	56.23		1.37795		72.7	41.2	59.6
2	1	4	57.36		1.36022		38.0	16.7	28.9
3	0	3	57.38		1.36001		.0	.0	.0
2	2	0	59.08	59.08	1.33525	4.7	433.3	407.9	423.5

Table 2b. Powder X-ray Diffraction Diagram of $Dy_{.333}Fe_{.317}Al_{.30}$

Material: Induction Melted

Radiation: CrKα

Structural Data: $MgZn_2$ Type, Hexagonal a = 5.348Å c = 8.695Å

Space Group: No. 194, D_{6h}^4 - $P6_3/mmc$

Atomic Positions:

4f 1/3, 2/3, z (z = 1/16)
2a 0, 0, 0
6h x, 2x, 3/4 (x = 1/6)

Calculated Ordering Schemes

	Ordering 1	Ordering 2	Ordering 3 (stat).
4f	100% Dy	100% Dy	100% Dy
2a	100% Fe	100% Al	55% Fe, 45% Al
6h	10% Fe, 60% Al	73% Fe, 27% Al	55% Fe, 45% Al

h	k	ℓ	$\theta_{calc.}$	$\theta_{obs.}$	$d_{calc.}$	Relative Intensity $I_{obs.}$	I_{calc} Ord. 1	I_{calc} Ord. 2	I_{calc} Ord.3(stat)
1	0	0	14.32	14.32	4.63150	2.5	199.3	340.2	259.1
0	0	2	15.28	15.35	4.34750	1.5	249.6	85.5	163.9
1	0	1	16.27	16.35	4.08775	2	240.4	170.3	206.9
1	0	2	21.18	21.20	3.16979	2	133.5	285.1	195.8
1	1	0	25.36	25.42	2.67400	7.5	875.7	633.1	759.9
1	0	3	27.79	27.80	2.45691	10	1000.0	1000.0	1000.0
2	0	0	29.65	29.70	2.31575	1.8	131.2	203.8	162.4
1	1	2	30.19	30.24	2.27765	9	984.2	812.2	903.5
2	0	1	30.79	30.85	2.23774	4	383.8	459.4	417.5
0	0	4	31.80	31.80	2.17375	0.5	41.5	39.1	40.4
2	0	2	34.09		2.04387		.0	1.1	.2
1	0	4	35.60		1.96779		35.0	14.8	24.7
2	0	3	39.28	39.30	1.80918	1	115.5	75.8	96.3
2	1	0	40.87	40.90	1.75054	0.5	31.0	48.8	38.6
2	1	1	41.87	41.90	1.71611	0.5	44.4	32.6	38.8
1	1	4	42.77		1.68673		1.2	1.7	.0
1	0	5	44.72	44.72	1.62802	2	186.0	162.0	174.8
2	1	2	44.86		1.62384		43.0	84.7	60.3
2	0	4	46.28		1.58489		.0	7.0	1.6
3	0	0	47.90	47.90	1.54383	2	195.8	144.5	171.4
3	0	1	48.90		1.52006		.0	.0	.0
2	1	3	49.86	49.86	1.49844	5.5	559.5	557.1	558.4
3	0	2	51.94	52.03	1.45482	3	335.9	279.4	309.4
0	0	6	52.22		1.44916		44.6	60.5	51.5
2	0	5	55.46	55.46	1.39057	4.5	418.0	449.9	432.4
1	0	6	55.92		1.38304		74.5	42.4	58.7
2	1	4	57.15		1.36340		36.8	15.9	26.2
3	0	3	57.21		1.36258		.0	.0	.0
2	2	0	58.95	58.96	1.33700	4	421.2	396.3	409.7

Table 2c. Powder X-ray Diffraction Diagram of $Dy_{.333}Fe_{.317}Al_{.35}$

Material: Induction Melted and annealed (250 hrs 1000°C)

Radiation: CrKα

Structural Data: $MgZn_2$ Type, Hexagonal a = 5.392Å c = 8.711Å

Space Group: No. 194, D^4_{6h} - $P6_3/mmc$

Atomic Positions:

4f	1/3, 2/3, z (z = 1/16)
2a	0, 0, 0
6h	x, 2x, 3/4 (x = 1/6)

Calculated Ordering Schemes:

	Ordering 1	Ordering 2	Ordering 3 (Stat.)
4f	100% Dy	100% Dy	100% Dy
2a	100% Fe	100% Al	48% Fe, 52% Al
6h	30% Fe, 70% Al	63% Fe, 37% Al	48% Fe, 52% Al

h	k	ℓ	$\theta_{calc.}$	$\theta_{obs.}$	$d_{calc.}$	Relative Intensity $I_{obs.}$	$I_{calc.}$ Ord. 1	Ord. 2	Ord.3 (stat)
1	0	0	14.20	14.25	4.66960	2.5	176.8	300.5	238.5
0	0	2	15.25	15.32	4.35550	1.5	235.2	87.1	147.5
1	0	1	16.16	16.20	4.11557	2.0	220.8	159.1	186.7
1	0	2	21.08	21.12	3.18506	2.0	108.1	235.8	169.9
1	1	0	25.14	25.17	2.69600	6.5	763.7	556.4	649.4
1	0	3	27.68	27.70	2.46582	8.3	829.2	834.2	831.8
2	0	0	29.38	29.41	2.33480	1.5	106.0	167.9	137.2
1	1	2	29.98	29.96	2.29237	7	823.1	682.0	746.4
2	0	1	30.53	30.59	2.25520	3	303.9	369.1	337.7
0	0	4	31.73	31.75	2.17775	0.4	31.4	29.7	30.5
2	0	2	33.82		2.05778		.0	1.7	.6
1	0	4	35.48		1.97366		28.4	11.8	18.7
2	0	3	39.02	39.0	1.81954	1	107.9	72.5	88.2
2	1	0	40.47	40.5	1.76494	0.5	27.4	42.9	35.2
2	1	1	41.47	41.5	1.72979	0.5	40.5	30.1	34.8
1	1	4	42.54		1.69409		1.4	1.1	.0
2	1	2	44.45	44.53	1.63574		35.0	70.2	52.2
1	0	5	44.57		1.63229	2.0	159.7	140.0	149.1
2	0	4	45.99		1.59253		.0	4.0	1.2
3	0	0	47.38	47.42	1.55653	1.5	168.1	125.0	144.4
3	0	1	48.38		1.53226		.0	.0	.0
2	1	3	49.42	49.5	1.50819	4.5	461.9	462.6	462.3
3	0	2	51.40	51.4	1.46574	2.5	276.3	230.8	251.6
0	0	6	52.09		1.45183		35.0	48.3	41.8
2	0	5	55.12	55.12	1.39631	3.5	333.8	362.2	348.7
1	0	6	55.71		1.38637		63.3	36.4	48.1
3	0	3	56.61		1.37185		.0	.0	.0
2	1	4	56.66		1.37117		29.4	12.5	19.6
2	2	0	58.18	58.18	1.34800	3.2	334.7	316.7	325.1
3	1	0	62.18		1.29511		26.0	39.0	32.6
3	3	3	62.81		1.28773	0.6	103.2	45.5	69.6
3	1	1	63.40		1.28103		38.8	29.3	33.6
1	1	6	63.65	63.65	1.27826	0.8	64.3	78.4	71.6
3	0	4	64.76		1.26633		1.3	1.0	.0
3	1	2	67.33		1.24139		46.7	89.3	67.6
2	1	5	67.49	67.50	1.23988	4.0	403.4	355.0	377.3
2	0	6	68.29	68.30	1.23291	2	196.2	162.9	178.1
1	0	7	72.29	72.30	1.20246	1	92.2	97.9	95.2
3	1	3	75.56	75.55	1.18279	10	1000.0	1000.0	1000.0

show comparable intensities). No deviations from the situation of statistical distribution of Fe and Al are found for $Dy_{.333}Fe_{.333}Al_{.333}$ for a melted only material. $Dy_{.333}Fe_{.317}Al_{.350}$ melted only seems to contain minor impurities of C15 type since the prism planes (220 for instance) are slightly more diffuse than planes that do not appear in both C15 and C14 type. Moreover, the intensities observed deviate somewhat from any of the 3 calculated ones. (The prism planes are somewhat too strong.) The annealed material $Dy_{.333}Fe_{.317}Al_{.35}$, however, is well behaved and suggests again statistical order. (There is, maybe, a slight tendency toward a preference of Al for 2a sites.)

Magnetic information is summarized in table 3. Saturation moments at cryogenic temperatures (4.2K) oscillate in a manner reminiscent of a sine wave over the region of concentration. There is first a marked increase on substitution by Al, then a decrease and finally a strong rise to $9.3\mu_B$ for $DyAl_2$. Remanences, irrespective of crystal structure follow roughly the saturation moments, save for the region of concentration close to $DyAl_2$ where they drop considerably.

The most interesting observation may concern the mechanism of saturation at cryogenic temperatures. Figures 1a-k show the dependence of magnetization on the field. The general trend in the intermediate region of composition is one of developing S-type saturation behavior at the lowest temperatures. In many instances, partly at 4.2K but mostly at 1.6K, spontaneous increases in magnetization with field are observed which can cover a major portion of the magnetization at saturation. At still higher fields the magnetization

Table 3 Magnetic Parameters of $DyFe_2$-$DyAl_2$ and $DyCo_2$-$DyAl_2$

Composition $Dy_{.333}Fe_{.667-x}Al_x$		n_B (Saturation Moment per formula unit)	Remanence (Bohr Magnetons)	Temperature (°K)
x =	.00	5.805		1.6
		5.870	3.20	4.2
		5.870		10
		5.793		20
	.05	6.375		1.6
		6.365	4.92	4.2
		6.195		10
		6.142		20
		6.152		40
	.10	6.910		1.6
		7.315	5.10	4.2
		6.972		10
		6.386		20
	.15	7.845	5.31	4.2
		6.560		20
	.20	8.080	5.26	4.2
		6.990		20
	.25	7.450		1.6
		7.525	4.575	4.2
		6.955		20
	.30	7.320		1.6
		7.500	4.53	4.2
	.35	6.830		1.6
		7.080	4.06	4.2
	.45	6.745	3.630	1.6
		6.785	3.730	4.2
		6.525	2.675	10
	.50	6.88		
		6.76	3.35	4.2
		6.53	1.25	10

Composition	n_B	Remanence	Temperature
x = .55	6.808		1.6
	6.820		4.2
.60	7.800	3.50	1.6
	7.590	2.62	4.2
	7.525		20
.65	9.150		1.6
	9.140	2.775	4.2
	7.180		20
.667	9.325		1.6
	9.130	.605	4.2
$Dy_{.333}Co_{.667-x}Al_x$			
x = .00	7.6[1]		4.2 (T_c=159K)[1]
.333	6.82	1.44	4.2
.417	6.56	0.95	4.2
.492	6.82	1.23	4.2
.567	7.76	1.02	4.2
.667	9.13	0.605	4.2

(1) Figure taken from J. Farrel and W.E. Wallace, Inorg. Chem., 5, 105 (1966). T_c = Curie temperature.

is rising almost linearly, so that in fact the saturation moments determined from this region will have only a limited meaning. After exposure to fields a relatively high remanence is left, and no abnormalities are observed on a second experiment with increasing fields. In most instances the effect is repeatable if the material is heated beyond its ordering temperature and cooled in the absence of a field, see Fig. 16. In some cases, however, only the pronounced S-type behavior was observed, and this particularly after aging of the material for several months (see Fig. 1d). The powder size may have varied from 50-300 mesh in various cases but no obvious dependence on the powder size was observed in experiments on materials with different powder size.

The magnetic behavior of $DyCo_2$-$DyAl_2$ is included in Table 2 and Fig. 1. This investigation was only orienting in nature but showed a similar behavior to $DyFe_2$-$DyAl_2$ with the exception that no discontinuous increases in magnetization with field were found. The composition $Dy_{.333}Co_{.10}Al_{.567}$ shows the characteristic, almost linear increase in magnetization beyond persuasive signs of saturation that has been observed invariably in materials where a transition metal replaces Al in the rare earth dialuminides.

DISCUSSION

The succession of crystal structures from the $MgCu_2$ type to $MgZn_2$ and back again to $MgCu_2$ is the rule in systems involving dialuminides of heavy rare earths where Al is replaced by Co[36] or Fe[37] (with exception of YbFeAl which is not $MgZn_2$ type). The first structural breakdown can be explained in terms of Fermi-surface-Brillouinzone interactions as a consequence of the changing e.c., and this may also hold for the electron rich phase boundaries. From a comparison of the Gd, Tb, Dy and Er systems it appears that the phase boundaries are somewhat shifted to lower Al concentrations the heavier the lanthanide in question.

The increase in saturation moment at 4.2K on initial Al substitution for Fe in $DyFe_2$ in all likelihood is caused by the replacement of a non-magnetic entity for a magnetic (Fe) which is aligned antiparallel to the rare earth. The increase, however, is more pronounced than would be expected from the decreased competition between transition metal and rare earth moment. This indicates moment quenching on Fe probably due to enhanced electron transfer to Fe 3d bands as a consequence of the rising e.c. on Al addition. An extrapolation of the saturation moments to $10\mu_B$ (the theoretical saturation moment of $DyAl_2$) versus composition indicates that beyond an approximate composition $Dy_{0.333}Fe_{0.277}Al_{.39}$ Fe would be nonmagnetic. Although this is a somewhat uncertain procedure especially when viewed in the light of the magnetic complexities outlined below, similar results were obtained in

$GdFe_2$-$GdAl_2$ and $ErFe_2$-$ErAl_2$ where the situation is either more straightforward or where we had additional information from the paramagnetic region.

The situation in C14 DyFeAl and C15 $DyAl_2$(Fe) is best considered in comparison with the neutron diffraction studies on $ErCo_2$-$ErAl_2$[19]. There we have shown that the rare earth sublattice moment decreases dramatically from a value of $8.83\mu_B$ for $ErAl_2$ to values as low as 4 or $5\mu_B$ in the intermediate region. A similarly dramatic rise in the diffuse background scattering shows that this moment is not lost but disordered. It is plausible that the relatively low saturation moments in $DyFe_2$-$DyAl_2$ are also the result of the development of partial magnetic disorder. Our intensity study may, in fact, more or less relate this disorder to the disorder on crystallographic sites, since the tendency toward more complete magnetic order in the direction of decreasing Al content in C14 $DyFe_xAl_{1-x}$ coincides with a slight tendency for crystallographic ordering between Fe and Al. The disorder between Fe and Al in C15 $DyFe_2$(Al), on the other hand, does not seem to have a similar influence, and it remains somewhat questionable, therefore, what causes the depression in saturation moments around the composition $Dy_{.333}Fe_{.167}Al_{.50}$. The linearly increasing magnetizations at the highest fields appear to indicate either the ordering of disordered components into the field direction similar to the situation in $ErCo_2$-$ErAl_2$ or else point at the presence of strong anisotropy or domain effects. Crystal field effects are not a likely source, considering the analogy to $ErCo_2$-$ErAl_2$.

In the absence of additional information from either neutron diffraction or Mössbauer spectroscopy, the unusual stepwise increases of magnetization with field will again best be viewed in the light of earlier investigations. The presence of similar although less pronounced discontinuities in $ErCo_2$-$ErAl_2$ for which we had additional neutron evidence for complete ferromagnetism, suggests domain wall effects as the origin,[38] rather than metamagnetism. This is also plausible in the light of the high remanences. A relation to the high anisotropies which in turn may be caused by the crystallographic disorder also suggests itself. A detailed understanding of this effect, however, is still wanting.

A similar effect in Dy_3Al_2[23] was explained as originating from domain walls of atomic dimensions as a result of the canted moment structure. It is possible that the presence of disordered components can play a similar role causing characteristic domain walls which will break down at critical fields. The most obvious model that comes to mind for one kind of characteristic domain wall is one of atomic dimensions. Since the thickness of a domain wall in a straightforward model[39] is determined by the counterplay of exchange energy E_e (which tends to thicken the wall) and anisotropy energy E_A (which will constrict it), the total energy E_T of the wall will be $E_T = E_e + E_a \approx \frac{JS^2\pi^2}{Na^2} + KNa$ where J, N, K and a are the exchange integral, the number of atomic planes within the wall, the anisotropy constant and the lattice constant respectively. ~~Since~~ E_T will have a minimum with respect to N when $\frac{dE_T}{dN} = 0$, or $N = \left(\frac{JS^2\pi^2}{Ka^3}\right)^{1/2}$, which points out the characteristic

dependence of wall thickness on J and K. It appears that the anisotropy (K) seems to increase dramatically in the pseudobinary region especially at low temperatures. The lack of complete repeatability, however, suggests either damage being done to the crystals (fracture of crystals ?) on cycling from room to cryogenic temperatures or a borderline case where not in all instances is a domain structure formed with enough initial resistance of domain walls towards fields to create spontaneous responses.

On the other hand an avalanching effect within a spectrum of only relatively narrow domain walls cannot be ruled out either. In this model we would assume that this spectrum is resistant to high fields but that the eventual breakdown of certain regions takes along even larger ones. This has not to be of necessity a completely repeatable effect.

It is interesting to note that systems harboring the most pronounced spontaneous increases of magnetization with field so far found are Fe ones in preference to ones with Co, as well as Tb and Dy ones in preference to ones containing Ho and Er. The latter suggests that rare earth anisotropies will have to over-compensate for the decreasing exchange constants (3) which fall according to the deGennes function (together with the ordering temperatures) toward the heavier of the heavy rare earths. Gd analog alloys do show neither S-type behavior nor spontanieties in the saturation mechanism but this is not surprising in view of the S ground state of Gd^{3+}.

B. Studies on $TbFe_3Tb_2Fe_{17}$ with Substitution by Al for Fe:

Introduction: In a recent summary on studies of rare and transition metal Buschow[5] lists several intermetallic compounds with Tb and Fe, particularly $TbFe_3$($PuNi_3$ type) and Tb_2Fe_{17} (Th_2Ni_{17} type) and Tb_2Fe_{17} (Th_2Zn_{17} type). Aluminides $TbAl_3$ ($BaPb_3$ type)[40] or $PuAl_3$ type[41] are reported. Magnetic information is available for $TbAl_3$[44] and for the temperature dependence of $TbFe_3$[43] together with Tb_2Fe_{17}[46]. For the latter a saturation value of about $16\mu_B$ per mole is extrapolated for $0^\circ K$ and a temperature of $135^\circ C$ is found.

RESULTS AND DISCUSSION

Alloys have been prepared along pseudobinary segments $TbFe_3$-$TbAl_3$, Tb_2Fe_7-Tb_2Al_7, Tb_6Fe_{23}-Tb_6Al_{23}, $TbFe_5$-$TbAl_5$ and Tb_aFe_{17}-Tb_aAl_{17}. Only preliminary crystallographic studies were carried out to decide on the feasibility and interpretation of magnetic investigations. Exact phase relations and structural determinations are the subject of another study.[45].

Contrary to the expectation of compounds at compositions $TbFe_5$-$Tb(FeAl)_5$ and Tb_6Fe_{23}-$Tb_6(FeAl)_{23}$, the Debye Sherrer diagrams of melted and melted and annealed specimens showed these materials in a multiphase region. An exception occurs around a composition $Tb_{0.167}Fe_{0.633}Al_{0.20}$ where the Debye Scherrer diagram of melted and annealed specimens (200 hrs at 1000°C) show the presence of the Th_6Mn_{23} type. (See Table 4). Although considerable discrepancies in calculated and observed intensities exist between an ideal Tb_6Fe_{23} and $Tb_{.167}Fe_{.633}Al_{.20}$, we have assumed the latter to be of Th_6Mn_{23} type with ordering on crystallographic sites. This structure was first described by Florio et al.[4] with Th on 24e and Mn on 4b, 32f, 24d and 32f' (written in the order of decreasing volume of the crystallographic site in Th_6Mn_{23}). The intensities for several ordering schemes have been calculated and are compared in Table I with the ones observed. Intensity calculations were carried out with the free parameters of Th_6Mn_{23} according to $I = A.F.^2M.LP$ in which A, F, M and LP represent a scaling factor, the structure factor, the multiplicity and the Lorentz polarization factor respectively. We have used a program by Yvon et al.[5] for the computation. A calculation

Table 4. Powder X-Ray Diffraction Diagram of $Tb_{0.167}Fe_{0.633}Al_{0.20}$

Material: Induction Melted and Annealed for 200 hrs at 1000°C

Radiation: CrKα

Structural Data: Th_6Mn_{23} type, cubic face centered a = 12.173 Å

Space Group: No. 125, O_h^5 - Fm 3m

Atomic Positions:

24e	x,0,0 etc. (x = 0.203)
4b	1/2, 1/2, 1/2 etc.
32f	x, x, x etc (x = 0.378)
24d	1/4, 1/4, 0 etc
32f'	x, x, x etc (x = 0.178)

Calculated Ordering Schemes:

	Ordering 1[1)]		Ordering 2	
24e	81% Tb	19% Fe	53% Tb	47% Al
4b		100% Fe		100% Al
32f		100% Al		100% Fe
24d		100% Fe		100% Fe
32f'		100% Fe		100% Fe

(1) This computation was carried out for a fictitious G phase $Tb_{0.167}Fe_{0.583}Al_{0.25}$

h	k	ℓ	$\theta_{calc.}$	$\theta_{obs.}$	$d_{calc.}$	I_o	Calculated Intensity Ord.1		Ord.2	
1	1	1	9.38		7.02808		2.0		.1	
2	0	0	10.85	10.9	6.08650	1	80.0		130.3	
2	2	0	15.44	15.45	4.30380	1	93.3		6.0	
3	1	1	18.19		3.67029		.6		.8	
2	2	2	19.02	19.05	3.51404	3	159.0		83.5	
4	0	0	22.11	22.1	3.04325	3	230.4		65.3	
3	3	1	24.22	24.2	2.79267	2	518.4		154.3	
4	2	0	24.89	24.9	2.72196	0.5	25.7		12.7	
4	2	2	27.45	27.45	2.48480	5	315.9		312.4	
5	1	1	29.27	29.25	2.34269	8	500.0	775.5	512.4	872.5
3	3	3	29.27		2.34269		275.5		360.1	
4	4	0	32.16	32.2	2.15190	10	1000.0		1000.0	
5	3	1	33.83	33.8	2.05761	0.5	45.3		150.5	
4	4	2	34.37	34.4	2.02883	2	4.1	113.8	11.7	155.6
6	0	0	34.37		2.02883		109.7		143.9	
6	2	0	36.52		1.92472		4.6		75.0	
5	3	3	38.10		1.85636		7.3		114.1	
6	2	2	38.62		1.83514		2.9		51.3	
4	4	4	40.69		1.75702		13.6		4.5	
5	5	1	45.22	42.2	1.70456	2	108.2	152.8	82.6	118.8
7	1	1	42.22		1.70456		43.6		36.2	
6	4	0	42.73	42.7	1.68809	1	81.7		21.2	
6	4	2	44.76		1.62668		9.2		6.9	
5	5	3	46.28	46.3	1.58479	2	54.2	144.8	9.9	43.7
7	3	1	46.28		1.58479		90.6		33.8	
8	0	0	48.83	48.8	1.52162	3	114.2		63.6	
7	3	3	50.37	50.4	1.48716	4	321.0		213.4	
8	2	0	50.89		1.47619		2.4	15.7	2.9	6.1
6	4	4	50.89		1.47619		13.3		3.2	
6	6	0	52.98		1.43460	8	59.1	334.3	90.1	366.6
8	2	2	52.98	53.0	1.43460		275.2		276.5	
7	5	1	54.58	54.6	1.40561	3	39.1	211.6	48.9	225.7
5	5	5	54.58		1.40561		172.5		176.8	
6	6	2	55.12		1.39633		11.2		1.4	
8	4	0	57.31	57.3	1.36098	4	15.3		12.5	
7	5	3	59.01	59.0	1.33616	2	137.6	137.8	111.1	114.8
9	1	1	59.01		1.33616		.2		3.7	
8	4	2	59.59	59.6	1.32818	4	172.7		183.0	
6	6	4	61.97		1.29764		6.9		.4	
9	3	1	63.85	63.9	1.27607	1	36.8		120.2	
8	4	4	67.21	67.2	1.24240	9	410.7		477.4	
9	3	3	69.43	69.4	1.22343	8	312.8	550.6	471.4	634.6
7	7	1	69.43		1.22343		230.7		161.9	

Table (continued)

h k ℓ	$\theta_{calc.}$	$\theta_{obs.}$	$d_{calc.}$	I_o	Ord.1		Ord.2	
10 0 0	70.22	70.2	1.21730	7	144.0	157.2	100.3	240.3
8 6 0	70.22		1.21730		13.2		140.0	
10 2 0	73.66	73.7	1.19366	2	52.4	237.0	9.8	46.2
8 6 2	73.66		1.19366		184.6		36.4	
9 5 1	76.74	76.7	1.17680	10	708.6	1167.4	428.9	662.6
7 7 3	76.74		1.17680		458.8		233.7	
10 2 2	77.93	77.9	1.17134	2	49.6	243.8	96.5	417.9
6 6 6	77.93		1.17134		194.2		321.4	

(calculation I) was attempted according to the coordination number principle (large atoms in crystallographic sites of high coordination number) with a statistical distribution of Tb and Al on 24e and one between Fe and Al on the remaining crystallographic sites. This calculation suggests that the substance is of Th_6Mn_{23} type but with a somewhat different ordering. Another calculation (calculation II) with Tb and Al (80:20) in 24e. Al in 4b Fe in 32f and Fe and Al (70:30) in 32f and 24d shows better agreement.

Although no complete agreement between calculated and observed intensities could be obtained with the ordering schemes outlined in Table I, it seems clear that $Tb_{.167}Fe_{.583}Al_{.25}$ is of Th_6Mn_{23} type structure with some unusual ordering tendencies. Another ternary phase (induction melted only) is found around a composition $Tb_2(FeAl)_{17}$. It has so far been only identified as cubic body centered.[45]

$TbFe_3$ melted and melted and annealed crystallizes with the $PuNi_3$ type structure, as can be seen from a comparison of observed and calculated intensities of a D.S. diagram in Table 5. There is no appreciable change in intensity for $Tb_{0.25}Fe_{0.70}Al_{0.05}$, but $Tb_{0.25}Fe_{0.65}Al_{.10}$ seems to be a two phase material between two very closely related crystal structures. At higher Al concentrations a second phase seems to be pure beyond $Tb_{.25}FeAl_{.25}$ but $Tb_{.25}FeAl_{.30}$ is a multiphase material with C14 TbFeAl as major constituent. (lattice parameters are given in Table 6.) The major changes on the presumed crystallographic transformation appear in an addition of some new reflections and a pronounced change in the intensities of the fundamental pattern. Especially one line between 110 and 116 is successively increasing on Al

Table 5. Powder X-ray Diffraction Diagram of $TbFe_3$

Material: $TbFe_3$, Induction Melted Only

Radiation: Cr K α

Structural Data: $PuNi_3$-Type, Rhombohedral

$a = 5.135$Å $\quad c = 24.620$Å (for triple hexagonal unit cell)

Space Group: No. 166, D_{3d}^5 - R $\bar{3}$ m

Atomic Positions in the Triple Hexagonal Unit Cell:

Tb in 3a	0,0,0
Tb in 6c	0,0,z (z = 0.143)
Fe in 3b	0,0, 1/2
Fe in 6c	0,0,z (z = 0.3333)
Fe in 18h	1/2, 1/2, z (z = 0.0833)

h	k	ℓ	θ_{calc}	θ_{obs}	d_{calc}	Relative Intensity I_{obs}	Relative Intensity $I_{calc.}$	Relative Intensity $I(LaNi_3)_{calc.}$
0	0	3	8.02		8.20666		38.2	
1	0	1	15.17	15.2	4.37622	2	275.8	32.8
0	0	6	16.21	16.2	4.10333	1	58.9	63.4
1	0	4	18.53	18.5	3.60463	1	52.9	10.3
0	1	5	20.31		3.30030		.0	
1	0	7	24.53	24.5	2.75863	5	1000.0	406.7
0	0	9	24.75		2.73555		20.8	32.9
1	1	0	26.50	26.5	2.56750	5	548.7	923.0
0	1	8	26.91	26.9	2.53062	3	.1	282.3
1	1	3	27.87		2.45037		14.4	
0	2	1	31.15	31.1	2.21450	3	.0	344.1
2	0	2	31.57		2.18811		171.7	89.4
1	1	6	31.75	31.8	2.17654	10	929.4	2000.0
1	0	10	32.13	32.1	2.15393	0.5	65.7	38.9
0	2	4	33.21		2.09124		.0	99.3
0	0	12	33.94	33.9	2.05166	1	105.9	312.4
0	2	5	34.42	34.4	2.02648	1.5	211.5	141.6
1	0	11	34.96	35.0	1.99924	1.5	.0	120.9
0	2	7	37.55		1.87943		.0	1.0
1	1	9	37.72	37.7	1.87209	1	44.7	61.0
2	0	8	39.46		1.80231		52.9	
1	0	13	41.10		1.74242		15.0	
2	1	1	43.08		1.67692		48.9	14.0
0	0	15	44.26	44.3	1.64133	4	37.6	51.0
0	1	14	44.46		1.63534		.0	67.5
2	1	4	44.95		1.62145		13.0	
1	1	12	45.62		1.60279		12.6	
2	1	5	46.06		1.59070		.0	
2	0	11	46.56		1.57742		1.3	
2	1	7	49.05	49.0	1.51654	5	406.3	254.6
3	0	0	50.60	50.6	1.48234	2	132.9	165.7
1	2	8	50.94	50.9	1.47514	2	.0	
3	0	3	51.74		1.45874		31.3	
1	0	16	51.97		1.45415		.0	
0	2	13	52.61	52.6	1.44176	2	.0	90.8
2	0	6	55.25	55.25	1.39416	5	362.6	228.6
2	1	10	55.60		1.38816		52.8	35.8
1	1	15	55.92	55.9	1.38290	2	184.2	167.2
2	0	14	56.14	56.1	1.37931	5	406.8	108.4
0	1	17	56.29		1.37705		.0	5.2
0	0	18	56.87		1.36777		15.6	17.3

h	k	ℓ	θ_{calc}	θ_{obs}	d_{calc}	I_{obs}	$I_{calc.}$	$I(LaNi_3)_{calc.}$
1	2	11	58.46	58.5	1.34402	2	.0	123.2
3	0	9	61.51		1.30329		30.8	
2	2	0	63.16	63.1	1.28375	10	527.9	419.0
2	2	3	64.57		1.26832		5.2	
2	1	13	65.67		1.25711		34.4	
1	0	19	67.03		1.24405		.5	

Table 6. Structures and Lattice Parameters of $TbFe_3$-$TbAl_3$

Composition $Tb_{0.25}Fe_{0.75-x}Al_x$	Structure	a_o(Å)	c_o	c_o/a_o	Volume	Volume/ Atom
x=0.0 m)	$PuNi_3$	5.135	24.620	4.794	562.25	15.62
	$PuNi_3$	(5.122) 1)	(24.745) 1)	(4.831) 1)		
0.0	$PuNi_3$	5.135	24.629	4.796	562.47	15.62
0.05 m)	$PuNi_3$	5.160	24.781	4.803	571.55	15.88
0.05 a)	$PuNi_3$	5.159	24.771	4.801	571.00	15.86
0.10 m)	$PuNi_3$ 3)	5.168	24.867	4.812	575.07	15.97
0.10 a)	$PuNi_3$ 3)	5.170	24.863	4.809	575.63	15.99
0.15 m)	$(PuNi_3)$ 4)	5.189	24.950	4.808	581.79	16.16
0.15 a)	$(PuNi_3)$ 4)	5.189	24.974	4.813	582.37	16.18
0.20 m)	$(PuNi_3)$ 4)	5.211	25.113	4.819	590.58	16.41
0.20 a)	$(PuNi_3)$ 4)	5.211	25.113	4.819	590.58	16.41
0.25 m)	$(PuNi_3)$ 4)	5.226	25.191	4.820	595.80	16.55
0.25 a)	$(PuNi_3)$ 4)					
0.30 m)	$MgZn_2$ 3)	5.391	8.702	1.614	219.00	18.25
0.375 m)	$MgCu_2$ 3)	7.686			454.05	18.92
0.45 m)	$MgCu_2$ 3)	7.758			466.84	19.45
0.55 m)	$MgCu_2$ 3)	7.821			478.41	19.93
0.65 m)	$MgCu_2$ 3)	7.887			490.59	20.44
0.75 m)	$BaPb_3$	6.179 2) (6.175)	21.184 (21.180) 2)	3.428	700.45	19.46

m) Materials were induction melted only.

a) Materials were induction melted and annealed for about 200 hours at 1000°C.

1) Figures are taken for a more Fe rich multiphase material from K.H.J. Buschow, J.Less Comm.Metals, 11,204 (1966)

2) Figures are taken from J.H.N. VanVucht et al. J.LessComm.Metals, 10,98 (1965)

3) Multiphase material, Symbols represent major constituent.

4) Ternary phase (probably closely related to $TbFe_3$) Lattice Parameters were taken from 220 and 20,14 reflections of a presumed $PuNi_3$ type.

addition finally to become the strongest reflection at the highest Al contents. This is evident in the melted only specimen but most pronounced in the materials with successive heat treatment. The possibility of ordering between Fe and Al on different crystallographic site being responsible for the changes in intensity has been ruled out by an intensity calculation according to ordering schemes outlined in Table 7.

Tb_2Fe_7 may be of Ce_2Ni_7 type as can be seen from its Debye Scherrer diagram in Table 8. There are some minor discrepancies, however, and this question has to await final judgment at a later date. Similar changes in intensity are observed with Al concentration beyond $Tb_{0.222}Fe_{0.678}Al_{.10}$ as in the AB_3 compounds. An intensity calculation was carried out for $Tb_{0.222}Fe_{0.578}Al_{0.20}$ with various ordering schemes but failed to support the model of an Ce_2Ni_7 or any known related type, see Table 9. Lattice parameters under the assumption of a Ce_2Ni_7 type are summarized in Table 10.

Tb_2Fe_{17}, finally, crystallizes as Th_2Ni_{17} type from the melt only. Melted and annealed specimens (200 hrs at 1000°C) seem to be multiphase materials. This structure takes up Al beyond $Tb_{.106}Fe_{0.644}Al_{.25}$ with increasing lattice parameters (Table 11). An intensity calculation was attempted with different occupancy of Al and Fe on B sites and is presented in Table 12. This calculation suggests a state close to statistical order on B sites (ordering 3)

Magnetic studies were only carried out in the cryogenic region or at temperatures below 300K. Magnetic information is summarized in Table 13.

Table 7. Powder X-Ray Diffraction Diagram of $Tb_{0.25}Fe_{0.55}Al_{0.20}$

Material: Induction Melted (I), and Induction Melted and Annealed 200 hrs. at 1000°C (Ia) Respectively.

Radiation: CrKα

Structural Data: Calculated as $\underline{PuNi_3\ type}$, rhombohedral
a = 5.211 Å c = 25.113 Å

Space Group: No. 166, D_{3d}^5 - $R\bar{3}m$

Atomic Positions in the Triple Hexagonal Unit Cell:

3a	0, 0, 0
6c	0, 0, z (z = 0.143)
3b	0, 0, 1/2
6c'	0, 0, z (z = 0.3333)
18h	1/2, 1/2, z (z = 0.0833)

Calculated Ordering Schemes:

	Ordering 1 (Stat)	Ordering 2	Ordering 3
3a	100% Tb	100% Tb	100% Tb
6c	100% Tb	100% Tb	100% Tb
3b	73% Fe, 27% Al	100% Fe	20% Fe, 80% Al
6c'	73% Fe, 27% Al	100% Fe	20% Fe, 80% Al
18h	73% Fe, 27% Al	60% Fe, 40% Al	100% Fe

h k ℓ	$\theta_{calc.}$	$\theta_{obs.}$	$d_{calc.}$	Relative Intensity			
				$I_{obs.}$	Calculated Intensity		
					$I_{calc.}$ Ord.1	$I_{calc.}$ Ord.2	$I_{calc.}$ Ord.3
0 0 3	7.86		8.47100		50.0	42.6	64.1
1 0 1	14.94	14.9	4.44171	2	422.2	415.4	430.5
1 0 4	18.22		3.66440		64.8	80.3	42.0
1 0 7	24.07	24.1	2.80830	2	1000.0	1000.0	1000.0
0 0 9	24.24		2.79033		18.9	23.5	12.1
1 1 0	26.08	26.1	2.60550	7	526.9	665.1	324.7
1 0 8	26.39	26.4	2.57699	1	.0	.1	.0
1 1 3	27.41	27.4	2.48777	1	18.1	15.8	22.1
2 0 2	31.05	31.2	2.22085	10	140.5	141.2	138.2
1 1 6	31.19		2.21193		806.9	950.9	585.3
1 0 10	31.47		2.19441		59.2	63.0	53.0
0 0 12	33.18	33.2	2.09275	3	80.1	89.4	65.9
2 0 5	33.82	33.8	2.05826	0.5	144.1	155.2	125.3
1 1 9	36.98	37.0	1.90436	2	40.1	49.0	26.8
2 0 8	38.70	38.7	1.83220	0.5	65.8	81.9	42.1
1 0 13	40.17		1.77590		23.9	23.2	25.0
2 1 1	42.31	42.2	1.70177	1	68.8	69.2	67.6
0 0 15	43.17	43.2	1.67420	2	35.2	40.5	27.1
1 0 14	43.41		1.66693		.0	.1	.0
2 1 4	44.10		1.64603		15.1	18.5	10.2
1 1 12	44.59	44.6	1.63160	1	10.6	20.1	1.3
2 0 11	45.54		1.60484		.1	.6	5.4
2 1 7	48.04	48.05	1.54045	4	394.5	398.2	385.2
3 0 0	49.59	49.6	1.50428	5	123.6	154.7	77.9
1 0 16	50.59	50.6	1.48246	1	5.0	4.5	24.5
3 0 3	50.68		1.48057		27.7	29.5	5.9
1 1 14	50.83		1.47749		.0	.1	.0
2 0 13	51.31		1.46745		.0	.0	.0
3 0 6	54.01	54.0	1.41563	8	300.0	352.5	218.0
2 1 10	54.27		1.41100		45.3	48.4	39.8
1 1 15	54.41	54.6	1.40848	4	167.0	193.2	125.2
2 0 14	54.66		1.40415		352.4	378.3	306.9
0 0 18	55.19		1.39516		12.5	9.8	17.5
3 0 9	59.89		1.32412		25.6	31.3	17.0
2 2 0	61.55	61.55	1.30275	10	412.8	460.4	334.4
2 2 3	62.85	62.8	1.28725	0.5	5.8	5.2	6.8
2 1 13	63.62		1.27860		47.0	46.4	47.2
1 0 19	64.56		1.26845		.6	.0	4.1
3 1 2	66.88		1.24546		5.3	6.9	3.0
2 2 6	67.05	67.05	1.2438	3	50.7	84.6	12.6

Table 7. (continued)

h k ℓ	$\theta_{calc.}$	$\theta_{obs.}$	$d_{calc.}$	Relative Intensity			
					Calculated Intensity		
				$I_{obs.}$	$I_{calc.}$ Ord.1	$I_{calc.}$ Ord.ℓ	$I_{calc.}$ Ord.3
2 1 14	67.92		1.23608		.1	.1	.1
2 0 17	67.94	68.0	1.23593	3	243.1	265.7	200.5
1 1 18	68.64		1.22993		10.5	16.0	3.6
3 0 12	69.68		1.22147		14.5	27.2	1.9
3 1 5	70.59	60.6	1.21449	1	11.0	5.2	25.6
1 0 20	71.24		1.20969			.1	.1
0 0 21	73.31	73.3	1.19585	2		87.2	53.6
2 1 15	73.47		1.19481			.2	.1
2 2 9	76.02	76.0	1.18043	2		60.3	31.2

Table 8. Powder X-Ray Diffraction of Tb_2Fe_7

Material: Induction Melted

Radiation: Cr Kα

Structural Data: Ce_2Ni_7 Type, hexagonal a = 5.137 Å c = 24.481 Å

Space Group: No. 194, D^4_{6h}- $P6_3/mmc$

Atomic Positions:

Tb in 4f	1/3, 2/3, z (z = 0.03)
Tb in 4f	1/3, 2/3, z (z = 0.175)
Fe in 2a	0, 0, 0
Fe in 4e	0, 0, z (z = 0.167)
Fe in 4f	1/3, 2/3, z (z = 0.833)
Fe in 6h	x, 2s, 1/4 (x = 0.835)
Fe in 12h	x, 2x, z (x = 0.834, z = 0.085)

h	k	ℓ	θ_{calc}	θ_{obs}	d_{calc}	Relative Intensity $I_{obs.}$	$I_{calc.}$
0	0	2	5.37		12.241		19.8
0	0	4	10.79		6.12025		8.6
1	0	0	14.92		4.44877		43.3
1	0	1	15.17	15.2	4.37708	1	85.8
1	0	2	15.90		4.18118		5.9
0	0	6	16.30	16.3	4.08016	0.5	45.4
1	0	3	17.05		3.90602		18.7
1	0	4	18.56		3.59853		6.3
1	0	5	20.36		3.29260		1.9
0	0	8	21.98		3.06012		40.0
1	0	6	22.39		3.00699		117.8
1	0	7	24.62	24.6	2.74943	7	782.6
1	1	0	26.48	26.5	2.56850	5	581.1
1	0	8	27.02	27.05	2.52125	3	45.3
1	1	2	27.11		2.51375		5.4
0	0	10	27.90	27.8	2.44810	1	4.8
1	1	4	28.92	28.9	2.36838	1	9.6
1	0	9	29.58		2.32069		61.6
2	0	0	30.99		2.22438		143.7
2	0	1	31.14	31.1	2.21526	3	346.3
2	0	2	31.56		2.18854		.6
1	1	6	31.80	31.8	2.17366	10	1000.0
2	0	3	32.26		2.14608		78.3
1	0	10	32.28		2.14480		9.5
2	0	4	33.22		2.09059		.8
0	0	12	34.16		2.04008		124.5
2	0	5	34.44	34.4	2.02518	1	155.3
1	0	11	35.13	35.1	1.99038	1.5	74.6
1	1	8	35.61		1.96734		85.9
2	0	6	35.91		1.95301		20.6
2	0	7	37.61		1.87691		14.0
1	0	12	38.15		1.85440		23.6
2	0	8	39.54		1.79926		12.1
1	1	10	40.27		1.77210		21.0
0	0	14	40.92		1.74864		53.2
1	0	13	41.34		1.73418		40.6
2	0	9	41.70		1.72194		.0
2	1	0	42.94		1.68147		9.5
2	1	1	43.06		1.67752		14.6
2	1	2	43.44		1.66583		.7
2	1	3	44.07		1.64687		4.1
2	0	10	44.09		1.64630		2.6
1	0	14	44.74	44.7	1.62743	2	51.7
2	1	4	44.95		1.62139		1.9

h	k	ℓ	θ_{calc}	θ_{obs}	d_{calc}	I_{obs}	I_{calc}
1	1	12	45.81		1.59749		15.5
2	1	5	46.08		1.59031		.3
2	0	11	46.72		1.57328		2.0
2	1	6	47.46		1.55463		34.9
1	0	15	48.38		1.53221		12.7
0	0	16	48.47		1.53006		9.7
2	1	7	49.10	49.1	1.51542	4	322.5
2	0	12	49.63	49.8	1.50349	1	13.9
3	0	0	50.57	50.6	1.48292	3	139.9
3	0	1	50.70		1.48021		.1
2	1	8	51.01	51.0	1.47366	1	21.3
3	0	2	51.08		1.47216		1.6
3	0	3	51.73		1.45902		.0
1	0	16	52.34		1.44688		9.3
1	1	14	52.41	52.5	1.44545	2	191.5
3	0	4	52.63		1.44122		3.2
2	0	13	52.84		1.43726		236.2
2	1	9	53.21		1.43026		39.0
3	0	5	53.81		1.41925		.0
3	0	6	55.27	55.3	1.39372	7	389.7
2	1	10	55.73		1.38602		8.7
2	0	14	56.43	56.2	1.37471	7	60.8
1	0	17	56.73		1.37006		2.3
3	0	7	57.03		1.36526		.0
0	0	18	57.37		1.36005		9.0
2	1	11	58.63	58.6	1.34160	5	82.4
3	0	8	59.13		1.33448		49.8
2	0	15	60.52		1.31586		.4
1	1	16	60.62		1.31450		38.0
3	0	9	61.61		1.30200		.0
1	0	18	61.73		1.30063		3.8
2	1	12	61.98		1.29754		28.7
2	2	0	63.12	63.1	1.28425	9	589.2
2	2	2	63.74		1.27723		1.4
3	0	10	64.57		1.26857		18.8
2	0	16	65.32		1.26062		19.4
2	2	4	65.69		1.25687		2.5
2	1	13	65.96		1.25424		85.2
1	0	19	67.75		1.23761		17.5
3	0	11	68.15		1.23406		.0
3	1	0	68.18		1.23386		11.8
3	1	1	68.36		1.23230		21.7
3	1	2	68.91		1.22764		1.4
2	2	6	69.24		1.22500		37.3
0	0	20	69.36		1.22405		38.9

h	k	ℓ	θ_{calc}	θ_{obs}	d_{calc}	$I_{obs.}$	I_{calc}
3	1	3	69.87	69.8	1.22000	3	5.5
2	1	14	70.92	70.8	1.21203	3	158.5
3	1	4	71.27		1.20953		2.5
2	0	17	71.36		1.20884		46.0
			22.8			3	
			32.6			2	
			32.8			2	
			33.6			1	
			33.9			1	
			37.0			2	

Table 9. Powder X-ray Diffraction Diagram of $Tb_{0.222}Fe_{0.578}Al_{0.20}$

Material: Induction Melted

Radiation: Cr Kα

Structural Data: Calculated as Ce_2Ni_7 Type, hexagonal

a = 5.214 Å c = 25.086 Å

Space Group: No. 194, D^4_{6h} - $P6_3/mmc$

Atomic Positions:

4f	1/3, 2/3, z (z = 0.03)
4f'	1/3, 2/3, z (z = 0.175)
2a	0,0,0
4e	0,0,z (z = 0.167)
4f''	1/3, 2/3, z (z = 0.833)
6h	x, 2x, 1/4 (x = 0.835)
12ℓ	x, 2x, z (x = 0.834, z = 0.085)

Calculated Ordering Schemes

	Ordering 1	Ordering 2 (Stat)
4f	100% Tb	100% Tb
4f'	100% Tb	100% Tb
2a	28% Fe, 72% Al	74% Fe, 26% Al
4e	28% Fe, 72% Al	74% Fe, 26% Al
4f''	28% Fe, 72% Al	74% Fe, 26% Al
6h	100% Fe	74% Fe, 26% Al
12ℓ	100% Fe	74% Fe, 26% Al

h	k	ℓ	$\theta_{calc.}$	$\theta_{obs.}$	$d_{calc.}$	Relative Intensity $I_{obs.}$	$I_{calc.}$ Ord. 1	$I_{calc.}$ Ord. 2
0	0	2	5.24		12.53340		58.5	35.7
0	0	4	10.52		6.27150		20.3	14.4
1	0	0	14.69	14.8	4.51545	1	104.8	83.5
1	0	1	14.94	15.0	4.44403	1	174.0	157.4
1	0	2	15.64		4.24853		13.2	8.7
0	0	6	15.90	15.9	4.18100	1	7.9	72.4
1	0	3	16.76		3.97317		20.9	27.6
1	0	4	18.22		3.66445		12.9	9.1
1	0	5	19.95		3.35632		.9	2.3
0	0	8	21.43		3.13575		37.9	45.5
1	0	6	21.92		3.06784		205.3	141.7
1	0	7	24.08	24.1	2.80707	2	1000.0	901.6
1	1	0	26.06	26.1	2.60700	6	467.9	637.2
1	0	8	26.41		2.57560		44.7	49.7
1	1	2	26.66		2.55245		12.2	8.1
0	0	10	27.17		2.50860		3.7	5.4
1	1	4	28.41		2.40729		17.9	13.2
1	0	9	28.88		2.37183		70.4	67.3
2	0	0	30.49	30.5	2.25772	5	192.9	151.0
2	0	1	30.62	30.6	2.24864		439.4	352.6
2	0	2	31.03		2.22201		1.6	1.0
1	1	6	31.18	31.1	2.21218	10	866.7	1000.0
1	0	10	31.49		2.19290		8.2	10.0
2	0	3	31.70		2.17967		87.8	76.2
2	0	4	32.63		2.12426		1.9	1.4
0	0	12	33.23	33.2	2.09050	2	109.3	112.3
2	0	5	33.80		2.05887		147.0	136.7
1	0	11	34.24		2.03565		66.6	73.7
1	8	8	34.85		2.00467		83.3	93.5
2	0	6	35.21		1.98659		11.8	10.6
2	0	7	36.84	36.8	1.91024	1	24.2	32.1
1	0	12	37.14		1.89705		15.3	19.7
2	0	8	38.69		1.83222		11.6	13.6
1	1	10	39.32		1.80763		18.3	21.8
0	0	14	39.74		1.79185		56.7	59.3
1	0	13	40.20		1.77444		58.2	57.3
2	0	9	40.76		1.75440		.0	.5
2	1	0	42.16	42.2	1.70668	1	18.8	15.6
2	1	1	42.28		1.70274		26.8	24.9
2	1	2	42.64		1.69109		1.6	1.1
2	0	10	43.04		1.67816		1.9	2.8
2	1	3	43.24		1.67220		4.5	5.6
1	0	14	43.45		1.66551		54.3	58.6

h	k	ℓ	$\theta_{calc.}$	$\theta_{obs.}$	$d_{calc.}$	$I_{obs.}$	Ord. 1	Ord. 2
2	1	4	44.07		1.64679		3.4	2.5
1	1	12	44.61		1.63091		2.4	14.6
2	1	5	45.15		1.61575		.3	.4
2	0	11	45.55		1.60446		5.0	.9
2	1	6	46.46		1.58010		57.8	41.1
1	0	15	46.92		1.56829		13.9	13.2
0	0	15	46.93		1.56787		9.5	10.0
2	1	7	48.02	480.0	1.54087	2	390.6	355.3
2	0	12	48.31		1.53392		23.7	12.2
3	0	0	49.55	49.6	1.50515	4	111.6	148.6
3	0	1	49.68		1.50245		.1	.1
2	1	8	49.83		1.49903		20.0	22.4
3	0	2	50.04		1.49443		3.2	2.2
3	0	3	50.65		1.48134		.0	.0
1	0	16	50.66		1.48112		8.3	9.8
1	1	14	50.87		1.47668		191.4	207.3
2	0	13	51.34		1.46689		276.7	235.7
3	0	4	51.50		1.46359		5.4	4.1
2	1	9	51.90		1.45551		41.7	40.2
3	0	5	52.61		1.44167		.0	.0
3	0	6	53.98	53.9	1.41618	8	320.9	368.0
2	1	10	54.27		1.41108		7.1	8.4
2	0	14	54.70	54.6	1.40353	3	60.3	62.7
1	0	17	54.75		1.40264		5.1	2.5
0	0	18	55.28		1.39366		16.3	8.0
3	0	7	55.63		1.38772		.0	.0
2	1	11	56.96		1.36641		67.6	74.2
3	0	8	57.58		1.35693		44.7	49.8
2	0	15	58.47		1.34386		.5	.1
1	1	16	58.49		1.34360		33.0	38.2
1	0	18	59.33		1.33168		.9	3.6
3	0	9	59.87		1.32439		.0	.0
2	1	12	60.04		1.32205		16.0	21.3
2	2	0	61.49	61.5	1.30350	10	515.7	529.0
2	2	2	62.07		1.29651		2.8	2.0
3	0	10	62.56		1.29065		14.8	17.4
2	0	16	62.81		1.28780		16.5	17.8
2	1	13	63.64		1.27841		104.6	103.6
2	2	4	63.84		1.27622		4.4	3.4
1	0	19	64.67		1.26725		23.6	16.1
3	0	11	65.76		1.25621		.0	.0
0	0	30	65.95		1.25430		33.0	37.0
3	1	0	66.15		1.25236		20.0	17.1
3	1	1	66.32		1.25080		33.0	30.8
3	1	2	66.81		1.24616		2.5	1.7
2	2	6	66.99		1.24442		10.4	47.1

Table 10. Structures and Lattice Parameters of Tb_2Fe_7-Tb_2Al_7

Composition $Tb_{.222}Fe_{.778-x}Al_x$	Structure	a_o (Å)	c_o	c_o/a_o	Volume	Volume/ Atom
x = 0.00 m)	$(Ce_2Ni_7)^2$	5.137 (5.137)	24.481 (24.481)	4.766	559.37	15.54
0.00 a)	$(Ce_2Ni_7)^2$	5.142	24.735	4.810	566.38	15.73
0.05 m)	$(Ce_2Ni_7)^2$	5.153	24.520	4.758	563.99	15.67
0.05 a)	$(Ce_2Ni_7)^2$	5.164	24.893	4.821	574.85	15.97
0.10 m)	$(Ce_2Ni_7)^2$	5.177	24.607	4.753	571.56	15.87
0.10 a)	$(Ce_2Ni_7)^2$	5.182	24.924	4.810	579.59	16.10
0.15 m)	$(Ce_2Ni_7)^2$	5.194	24.929	4.800	582.39	16.18
0.15 a)	$(Ce_2Ni_7)^2$	5.199	24.920	4.793	583.28	16.20
0.20 m)	$(Ce_2Ni_7)^2$	5.214	25.086	4.811	590.72	16.41
0.20 a)	$(Ce_2Ni_7)^2$	5.213	24.919	4.800	586.55	16.29
0.25 m)	$(Ce_2Ni_7)^2$	5.221	25.084	4.804	592.13	16.448
0.25 a)	$(Ce_2Ni_7)^2$					
0.30 m)	$MgZn_2$ 3)	5.381	8.729	1.622	218.85	18.24
0.30 a)	$MgZn_2$ 3)	5.402	8.747	1.619	221.05	18.42
0.389 m)	$MgCu_2$ 3)	7.695			455.65	18.99
0.389 a)	$MgCu_2$ 3)	7.699			456.36	19.01

m) Materials were induction melted only

a) Materials were induction melted and annealed for about 200 hours at 1000°C

1) Figures are taken from K.H.J. Buschow, Phys. Stat. Solidi 7,199 (1971)

2) Purity and structural assignment may be questionable, however, the relationship to Ce_2Ni_7 seems to be a close one. Lattice parameters have been calculated according to the 220 and 21,14 reflections of a presumed Ce_2Ni_{17} type.

3) Multiphase material, symbols represent major constituent.

Table 11. Structures and Lattice Parameters of Tb_2Fe_{17}-Tb_2Al_{17}

Composition $Tb_{0.105}Fe_{0.895-x}Al_x$	Structure	a_o (Å)	c_o	c_o/a_o	Volume	Volume/Atom
x = 0.0	Th_2Ni_{17}	8.451	8.298	0.984	513.205	13.505
	Th_2Ni_{17}	(8.467)[4]	(8.309)[4]		(515.867)[4]	(13.575)[4]
0.05	Th_2Ni_{17}	8.465	8.320	0.983	513.26	13.586
0.10	Th_2Ni_{17}	8.506	8.342	0.981	522.79	13.758
0.15	Th_2Ni_{17}	8.532	8.349	0.978	526.70	13.86
0.25	Th_2Ni_{17}[2]	8.615	8.415	0.977	540.87	14.23
0.30						
0.4475	T[3]	8.657			648.78	
0.60	T[3]	8.729			665.11	

1) Materials were induction melted only.

2) Multiphase material, symbols represent major constituent.

3) Cubic body centered ternary phase

4) Figures are taken from K.H.J. Buschow, J.Less Comm. Metals, 11, 204 (1966)

Table 12. Powder X-Ray Diffraction Diagram of $Tb_{0.105}Fe_{0.745}Al_{0.15}$

Material: Induction Melted

Radiation: CrKα

Structural Data: $\frac{Th_2Ni_{17}\ type}{c=8.349\ Å}$, hexagonal $a=8.532\ Å$

Atomic Positions:

2b	0,0,1/4
2d	1/3, 2/3, 3/4
6g	1/2, 0,0
12j	x, 0, 1/4 (x = 1/3)
12k	x, 2x, 0 (x= 1/6)
4f	1/3, 2/3, z (z = 0.11)

Calculated Ordering Schemes:

Ordering 1	Ordering 2	Ordering 3(Fe, Al Statistical)
Tb 100% in 2b	Tb 100% in 2b	Tb 100% in 2b
Tb 100%in 2d	Tb 100% in 2d	Tb 100% in 2d
Fe43% in 6g;Al57% in 6g	Fe5.026% in 6g;Al94.974% in 6g	Fe83.24% in 6g;Al 16.76% in 6g
Fe 100% in 12j	Fe 100% in 12j	Fe83.24% in 12j;Al16.76% in 12j
Fe 100% in 12k	Fe 100% in 12k	Fe83.24% in 12k;Al 16.76% in 12k
Fe43% in 4f; Al57% in 4f	Fe 100% in 4f	Fe83.24% in 4f; Al 16.76% in 4f

Table 12. (continued)

h	k	ℓ	θ_{calc}	$\theta_{obs.}$	$d_{calc.}$	Relative Intensity $I_{obs.}$	$I_{calc.}$ Ord.1	$I_{calc.}$ Ord.2	$I_{calc.}$ Ord.3
1	0	0	8.92		7.38892		22.4	15.5	.2
1	0	1	11.95		5.53320		87.8	41.7	62.1
1	1	0	15.58	15.70	4.26600	0.7	23.1	78.9	68.4
0	0	2	15.93		4.17450		61.8	88.2	36.8
2	0	0	18.06		3.69446		.8	7.6	13.2
1	0	2	18.37		3.63455		20.2	14.5	45.8
2	0	1	19.82	19.90	3.37847	1	101.1	74.3	81.7
1	1	2	22.58	22.62	2.98364	4	393.0	359.1	460.7
2	1	0	24.21		2.79275		20.9	18.5	7.1
2	0	2	24.46		2.76660	0	114.3	181.7	57.8
2	1	1	25.63	25.65	2.64850	1	114.6	86.7	94.0
1	0	3	26.09		2.60439	0	58.9	89.6	87.9
3	0	0	27.71	27.80	2.46297	4	414.3	513.4	445.6
3	0	1	29.00		2.36232		.0	.0	.0
2	1	2	29.57	29.60	2.32120	0.5	34.6	29.8	55.1
2	0	3	31.02	31.05	2.22288	2	230.9	282.4	255.9
2	2	0	32.48	32.60	2.13300	10	441.6	464.0	546.0
3	0	2	32.68		2.12128		1000.0	1000.0	1000.0
0	0	4	33.28	33.25	2.08725	2.5	289.5	265.9	278.9
3	1	0	33.98		2.04932		.3	.1	.3
1	0	4	34.77		2.00864		17.4	28.7	17.1
3	1	1	35.14		1.99024		2.0	.2	1.2
2	1	3	35.53	35.4	1.97131	1	108.7	146.7	139.9
2	2	2	37.09	37.05	1.89941	2	116.1	101.1	124.5
1	1	4	37.66		1.87486		5.2	9.2	7.3
4	0	0	38.32		1.84723		4.9	12.3	1.3
3	0	3	38.39		1.84440		.0	.0	0.0
3	1	2	38.51		1.83960		1.7	.9	6.4
2	0	4	39.07		1.81727		12.6	9.1	32.1
4	0	1	39.43		1.80361		7.1	11.2	7.3
3	2	0	42.51		1.69513		11.0	10.4	5.8
4	0	2	42.69		1.68923		2.2	7.2	0.1
2	1	4	43.24		1.67189		37.0	54.6	36.1
3	2	1	43.59	43.60	1.66124	1	68.0	58.7	58.7
3	1	3	43.96		1.65018		15.9	26.8	28.4
1	0	5	44.69		1.62872		23.4	27.0	26.6
4	1	0	45.27	45.25	1.61239	1.5	12.8	24.8	22.2
3	0	4	46.00	46.00	1.59236	2	130.4	123.9	107.8
4	1	1	46.35		1.58314		.0	.0	0.0
3	2	2	46.83		1.57058		24.5	22.6	33.3

Table 12. (continued)

h	k	ℓ	θ_{calc}	$\theta_{obs.}$	$d_{calc.}$	Relative Intensity $I_{obs.}$	$I_{calc.}$ Ord.1	$I_{calc.}$ Ord.2	$I_{calc.}$ Ord.3
4	0	3	48.10		1.53905		14.1	20.9	21.2
2	0	5	48.83		1.52160		5.0	6.4	7.3
4	1	2	49.60	49.60	1.50409	3	165.9	156.2	190.1
2	2	4	50.16	50.15	1.49182	4	207.5	168.5	225.7
5	0	0	50.82		1.47778		4.4	4.2	
3	1	4	51.56		1.46231		11.1	19.9	
5	0	1	51.92		1.45516		29.7	25.9	
3	2	3	52.30	52.30	1.44772		102.8	129.7	
2	1	5	53.06	53.05	1.43316	0.3	76.6	86.2	
3	3	0	53.66	53.65	1.42200	1	84.1	105.3	
4	2	0	55.12		1.39637		.0	2.0	
4	1	3	55.19		1.39515		.0	.0	
5	0	2	55.31		1.39307		11.3	10.5	
0	0	6	55.40		1.39150		11.1	16.0	
4	0	4	55.90		1.38330		.0	.3	
3	0	5	55.97		1.38211		.0	.0	
4	2	1	56.27		1.37724		10.0	6.4	
1	0	6	56.89		1.36746		.7	.1	
3	3	2	58.32	58.30	1.34604	4	361.9	361.0	
5	1	0	59.67		1.32709		9.6	9.2	
4	2	2	59.88	59.95	1.32425	1.5	33.3	54.6	
1	1	6	59.98		1.32290		92.1	101.2	
3	2	4	60.52	60.80	1.31585	1	52.9	72.7	
5	1	1	60.92		1.31063		62.1	53.7	
5	0	3	61.36		1.30518		59.6	74.8	
2	0	6	61.60		1.30219		10.7	16.4	
3	1	5	62.23		1.29449		27.8	33.0	
5	1	0	59.67		1.27600			1.6	
4	2	2	59.88		1.26472			27.4	
1	1	6	59.98		1.24808			208.8	
3	2	4	60.52		1.24546			4.6	
5	1	1	60.92		1.23871			12.5	
5	0	3	61.36		1.23148			616.5	
2	0	6	61.60		1.21830			.0	
3	1	5	62.23		1.21473			2.7	
4	1	4	63.86		1.21151			818.6	

Table 13. Magnetic Parameters of $TbFe_3$-$TbAl_3$, Tb_2Fe_7-Tb_2-Al_7, Tb_2Fe_{17}-Tb_2Al_{17}

Composition[1] $Tb_{.25}Fe_{.75-x}Al_x$		n_B[2] Saturation Moment (Bohr Magnetons/ Norm.Form. Unit	Remanence (Bohr Magnetons)	Temperature °K
x =	.00[m]	.655	.311	4.2
			.298	20
			.293	40
			.279	80
			.203	180
			.193	260
	.05[m]	.861	.466	4.2
			.461	20
	.10[m]	1.058	.610	4.2
			.575	20
	.10[m]	.942	.543	4.2
	.15[m]	1.259	.766	1.6
			.722	4.2
			.654	20
			.598	40
			.468	80
			.258	180
			.184	260
	.15[a]	1.057	.684	1.6
			.684	4.2
			.628	20
			.564	40
			.455	80
			.340	160
			.176	260
	.20[m]	1.314	.817	4.2
			.751	20
			.645	40
			.522	80
			.307	180

Composition	n_B	Remanence	Temperature
.20[a]	1.266	.850	4.2
		.691	20
		.585	40
		.425	80
		.228	180
		.162	260
.25	1.371	.851	4.2
		.734	20
		.522	40
		.341	80
		.172	180
		.033	260

Composition[1] $Tb_{.222}Fe_{.778-x}Al_x$		n_B[2] Saturation Moment (Bohr Magneton/ Norm. Form. Unit)	Remanence (Bohr Magnetons)	Temperature (°K)
x =	.00[m]	.861	.288	4.2
			.266	20
	.05[m]	.847	.447	4.2
			.425	20
	.10[m]	1.020	.582	4.2
	.15[m]	.944	.585	4.2
			.514	20
			.505	40
			.422	80
			.183	260
	.15[a]	.866	.532	4.2
			.479	20
			.402	40
			.342	80
			.219	180
			.144	260
	.20[m]	1.053	.686	4.2
			.607	20
			.499	40
			.399	80
			.277	180
			.203	260
	.20[a]	.802	.513	4.2
			.412	20
			.340	40
			.295	80
			.221	180
			.137	260
	.25[m]	1.288	.774	4.2
			.741	20

Composition $Tb_{.105}Fe_{.895-x}Al_x$	n_B Saturation Moment (Bohr Magneton/ Norm.Form. Unit)	Remanence (Bohr Magnetons)	Temperature (^oK)
x = .00[m]	.988	.152	4.2
		.125	20
		.088	40
		.023	260
.05[m]	.742	.345	4.2
		.209	20
		.198	40
		.163	180
		.091	260
.10[m]	.698	.316	4.2
		.246	20
		.201	40
		.154	100
		.083	160
.15[m]	.521	.317	1.6
		.314	4.2
		.304	20
		.243	40
		.194	80
		.151	180
		.139	260
.4475[m]	.0397	.0013	4.2
		-.0013	20
		.0261	80
		.0456	180
		.0210	260
.60[m]	.402	.093	4.2
		.041	20
		-.007	40
		-.0012	80
$Tb_{.207}Al_{.793}$ annealed	.339		4.2

Composition	n_B	Remanence	Temperature
$Tb_{.167}Fe_{.633}Al_{.20}$ Annealed	.604	.349	412
		.303	20
		.235	40
		.223	80
		.178	180
		.073	260
$Tb_{.167}Fe_{.583}Al_{.25}$ Annealed	.554	.294	4.2

(1) m) Melted only material
a) Melted and annealed (about 200 hrs at 1000 K) material

(2) Normalized formula unit according to $Tb_xFe_yAl_z$ where $x + y + z = 1$. Saturation moments were extrapolated from curves of magnetic moment to zero reciprocal applied field.

h	k	ℓ	$\theta_{calc.}$	$\theta_{obs.}$	$d_{calc.}$	Relative Intensity $I_{obs.}$	I calc. Ord. 1	I calc. Ord. 2
3	1	3	67.64		1.23854		5.3	6.6
2	1	14	67.95		1.23582		138.0	147.8
2	0	17	68.02		1.23521		31.6	29.2
1	1	18	68.74		1.22906		38.7	57.1
3	1	4	68.86		1.22811		3.8	2.9
3	0	12	69.68		1.22148		3.4	19.4
3	1	5	70.51		1.21508		.1	.9
1	0	20	71.41		1.20854		89.7	94.1
				22.4		2		
				25.2		1		
				27.3		2		
				33.2		3		
				49.0		3		
				57.3		3		

The relatively low saturation moments especially at cryogenic temperatures suggest antiparallel alignment between Fe and Tb sublattices at all compositions investigated. This results in generally rising magnetizations at higher temperatures and anticipated compensation points at still higher ones. Remanences follow generally the saturation moments. The individual field dependencies at different temperatures are shown in Figures 2a-n . Similar to the situation in $DyFe_2$-$DyAl_2$ spontaneous increases in magnetization with field are observed at the lowest temperatures (1.6K) in some three component materials. There is remarkably little difference in magnetic behavior within different crystal structures of similar composition, probably as a result of the close relationship of the latter.

V. SUMMARY

Crystallographic and magnetic behavior in the cryogenic region was studied for $DyFe_2$, $DyCo_2$, and $TbFe_3$-Tb_2Fe_{17} compounds with substitution for the transition metal by Al.

Unusual domain walls with high critical fields (up to 20 kOe) together with high anisotropies at low temperatures are observed, possibly as a result of the disorder between the transition metal and Al on crystallographic sites. A computer study of the line intensities in Debye Scherrer diagrams suggest that the tendency towards these unusual effects is less pronounced in regions of concentration with ordering tendencies on crystallographic sites.

All available evidence suggests that the coupling scheme between the rare earth and the transition metal moments stays an antiferromagnetic one at all investigated compositions. This results in compensation points and at high transition metal concentrations in relatively low saturation moments at cryogenic temperatures, often with dramatic increases with rising temperatures. Remanences are highest in regions of concentration with disorder on crystallographic sites and seem not to depend on the type of crystal structure.

VI. FIGURE CAPTIONS

Fig. 1 a-k. - Magnetization μ (Bohr magnetons per formula unit AB_2) versus applied field H (kOe) at different temperatures (k) for materials $DyFe_2$-$DyAl_2$.

Fig. 2 a - n. - Magnetization μ (Bohr magnetons per mean molecular weight $\bar{M} = A_x B_y Z_z$ where $x + y + z = 1$) versus applied field H (kOe) at different temperatures (K) for materials in the region of composition $Tb_{.25}Fe_{.75}$ to $Tb_{.105}Fe_{.895}$ with substitution for Fe by Al.

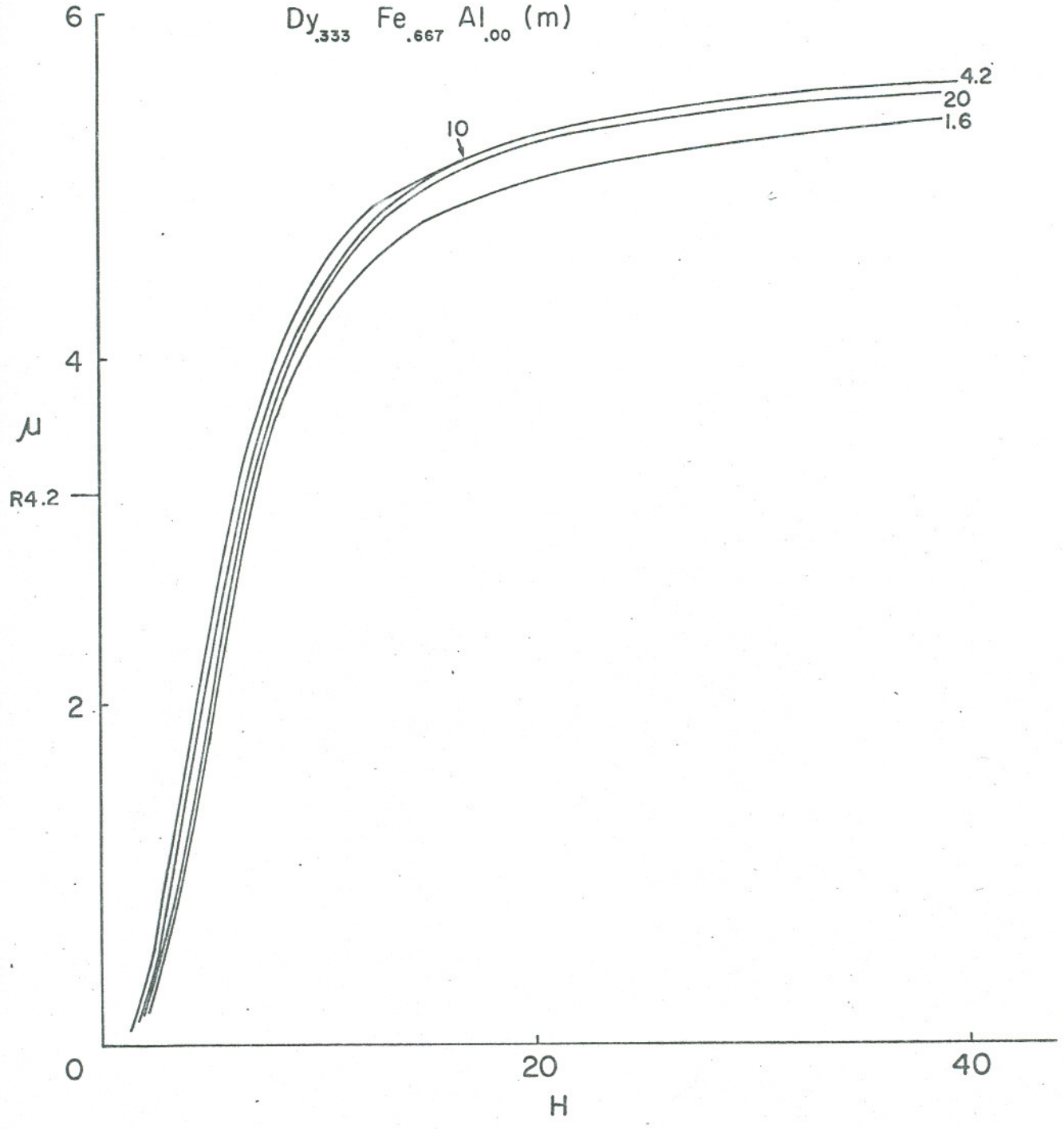

Fig 1a

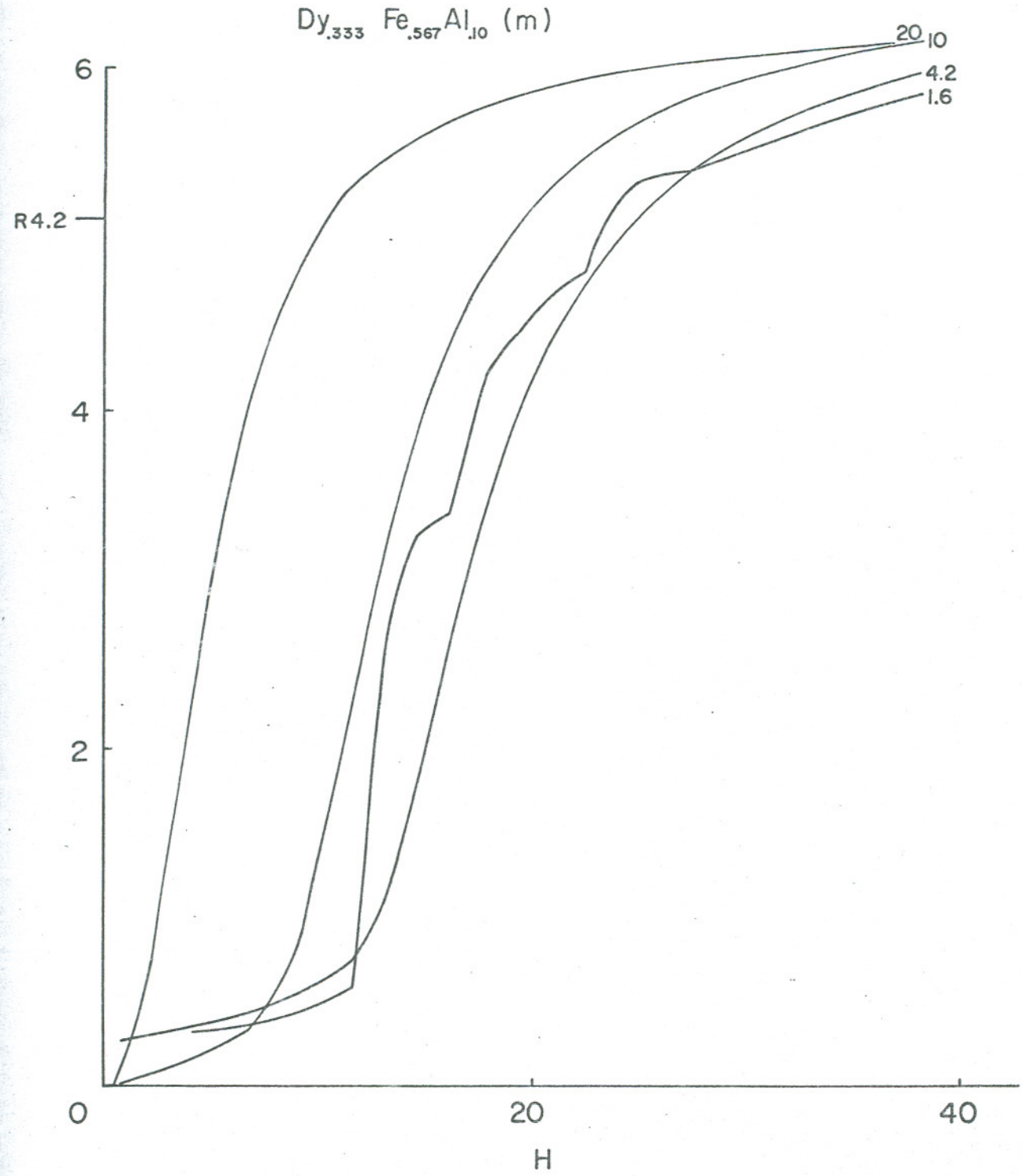

Fig 16

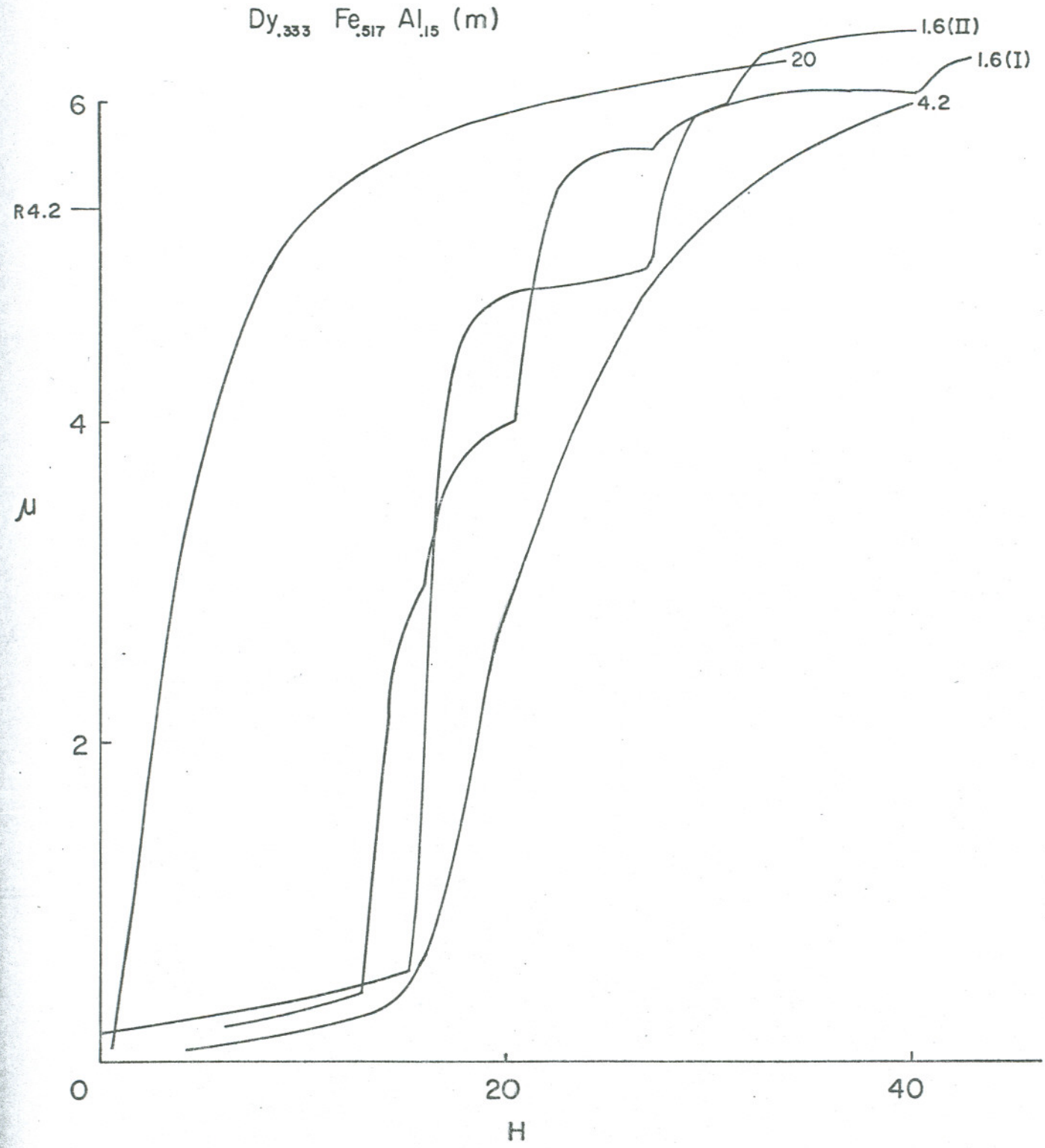

Fig. 1c

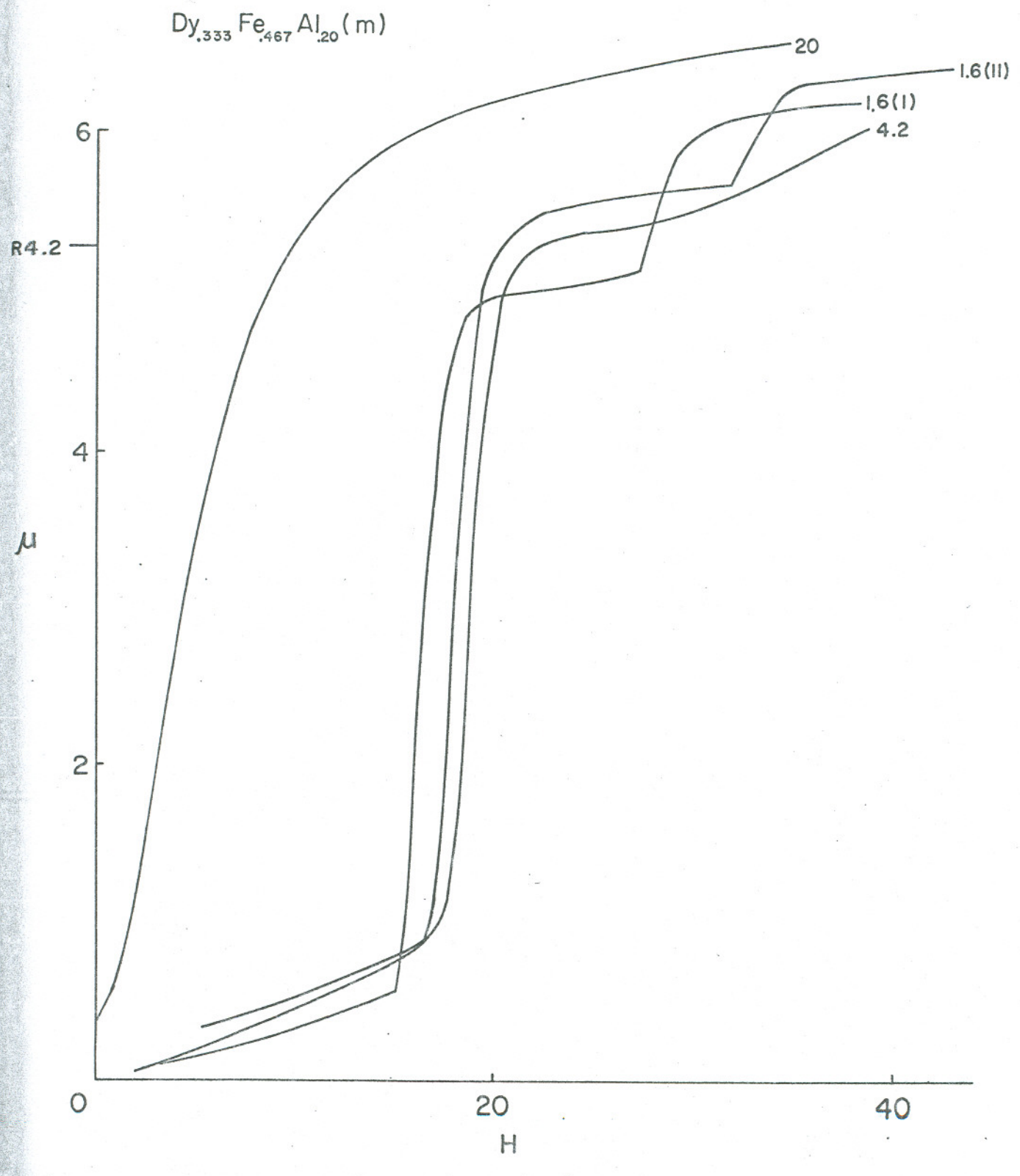

Fig 1d

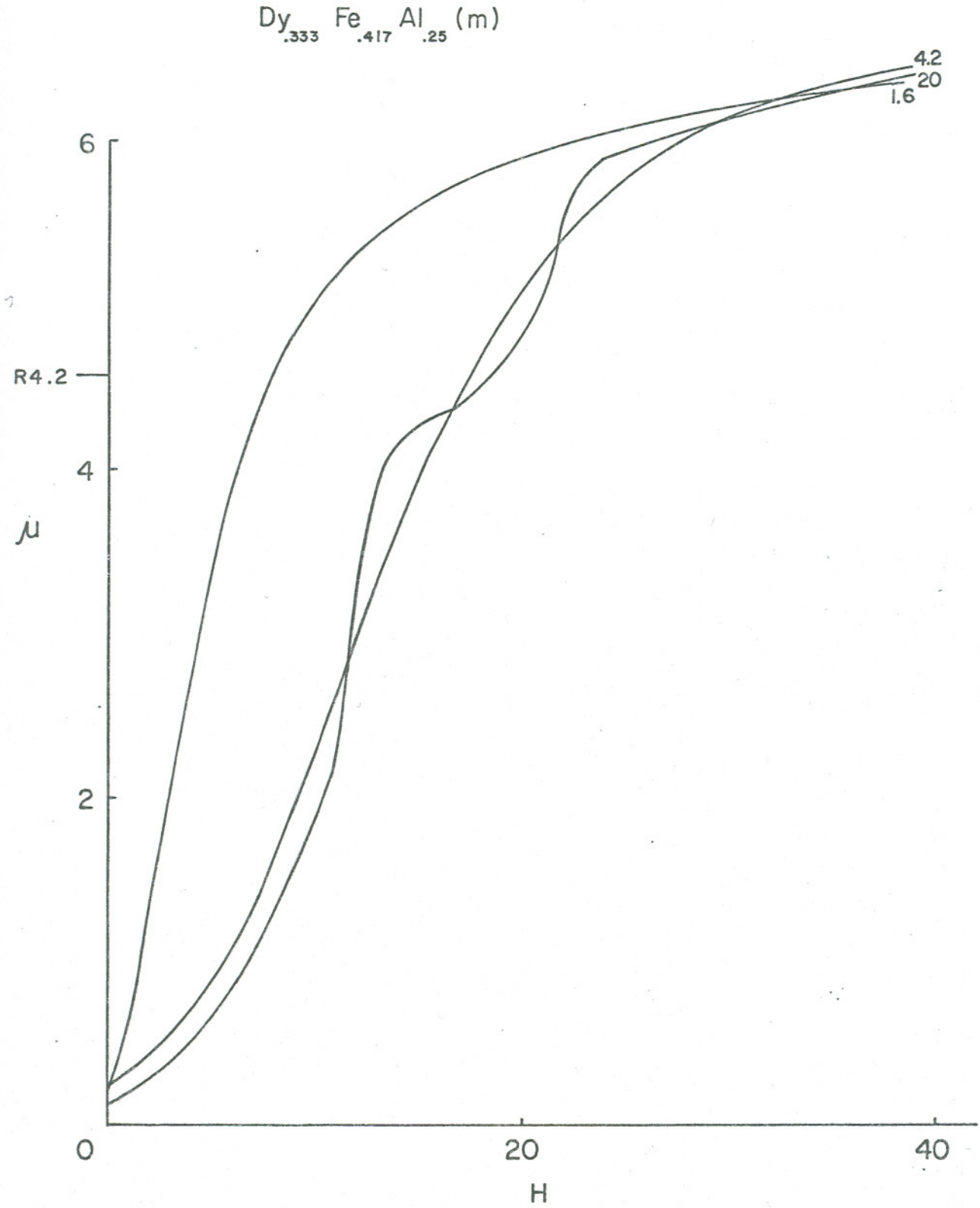

Fig 1e

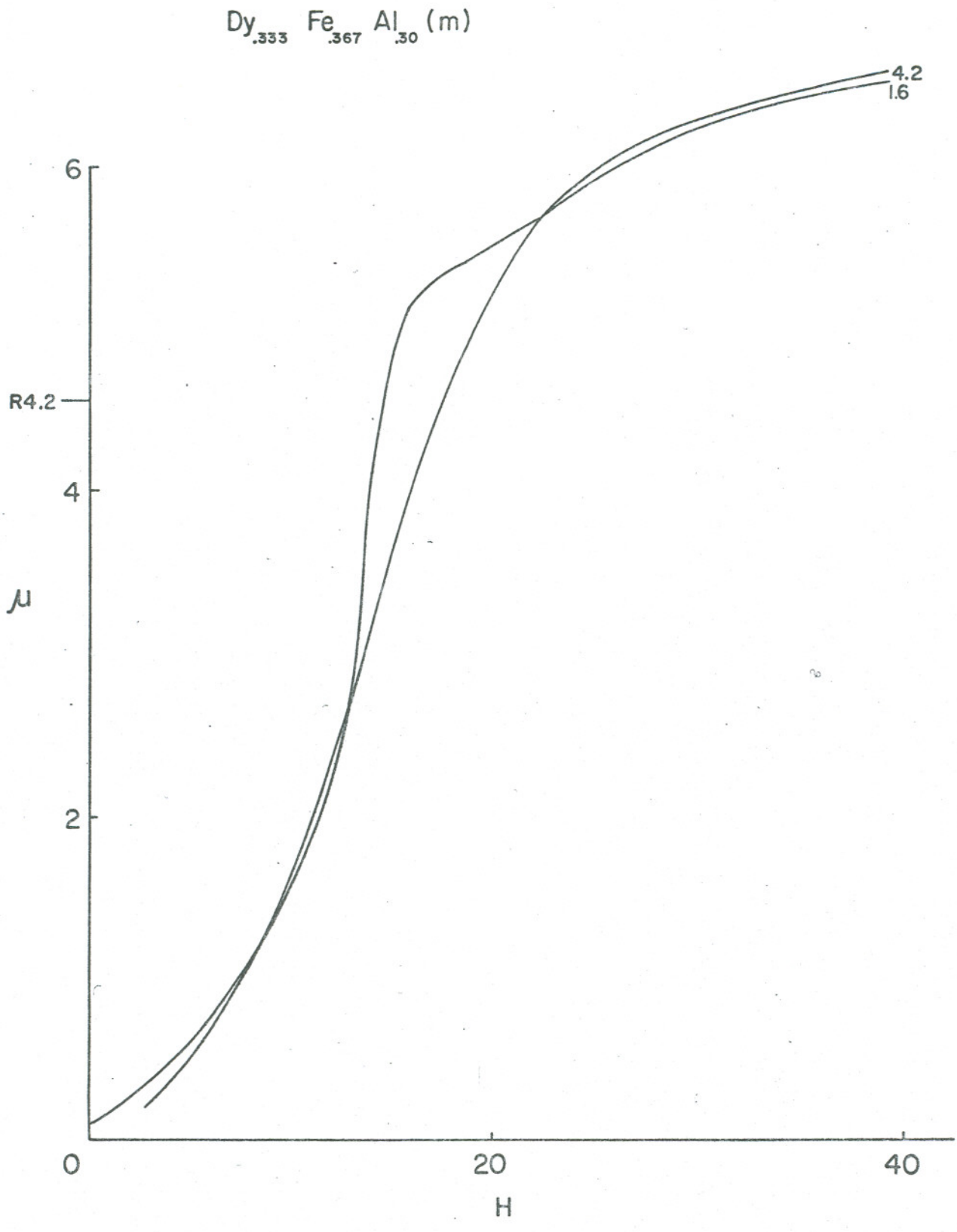

Fig 1 f

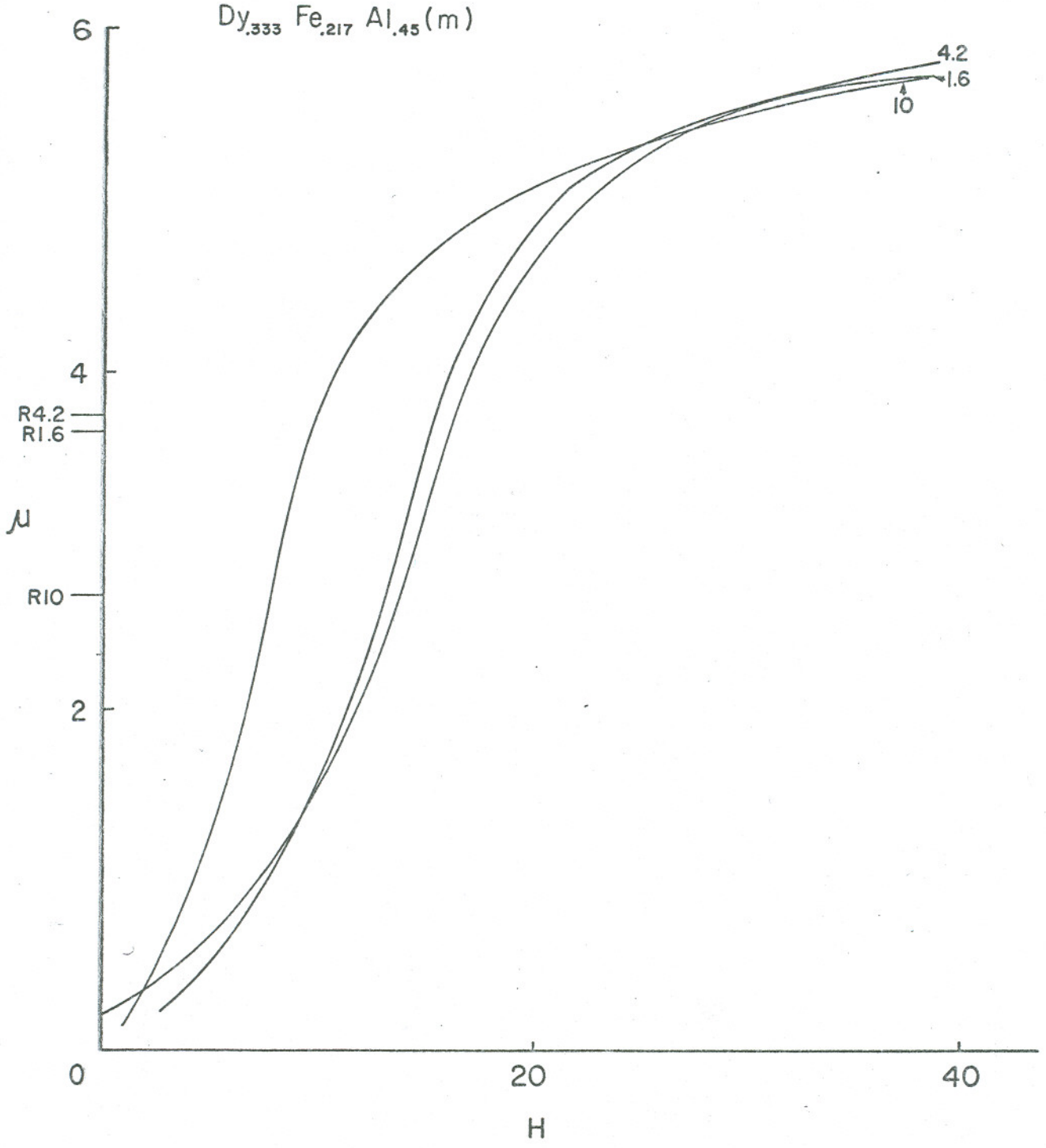

Fig 19

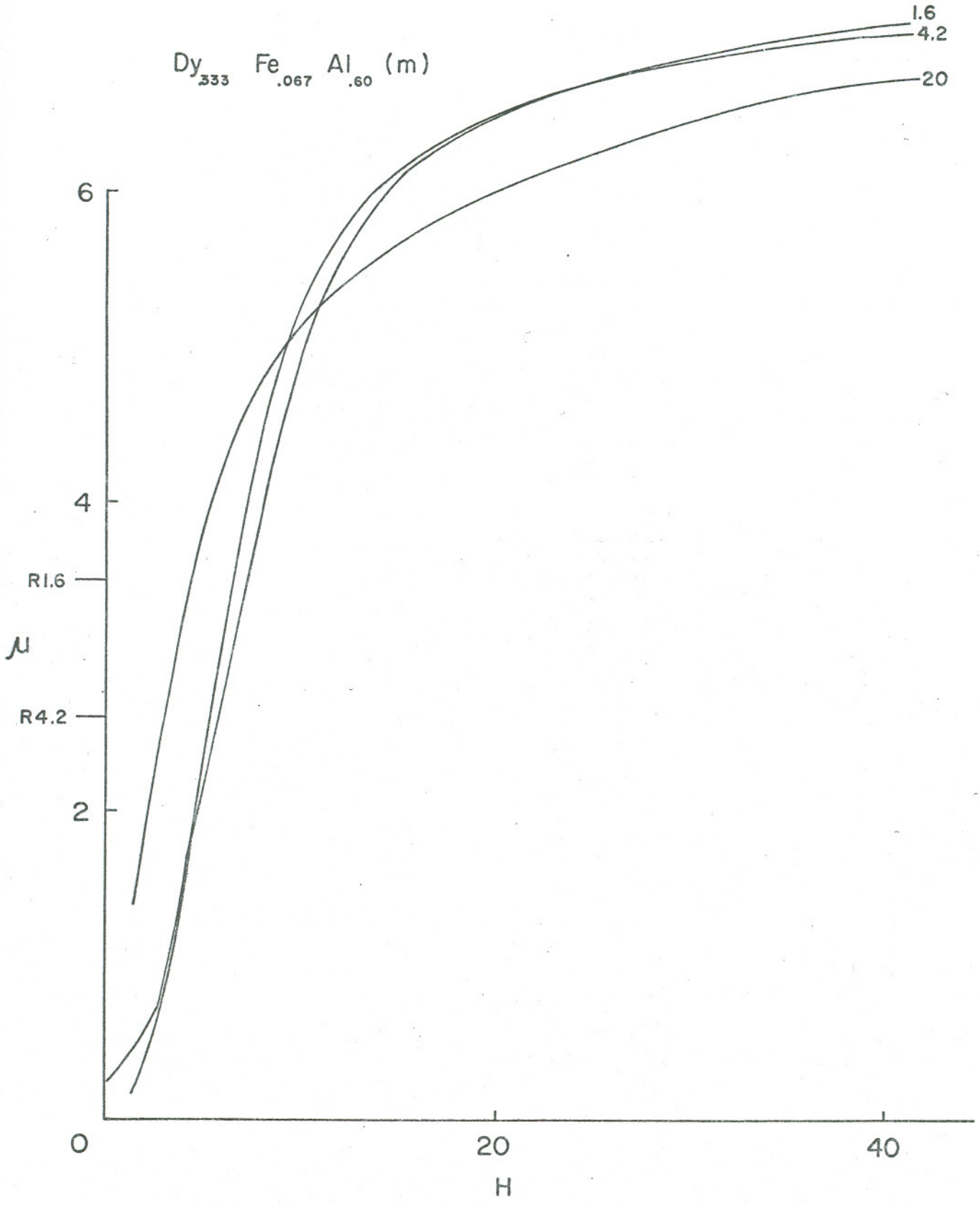

Fig 1 h

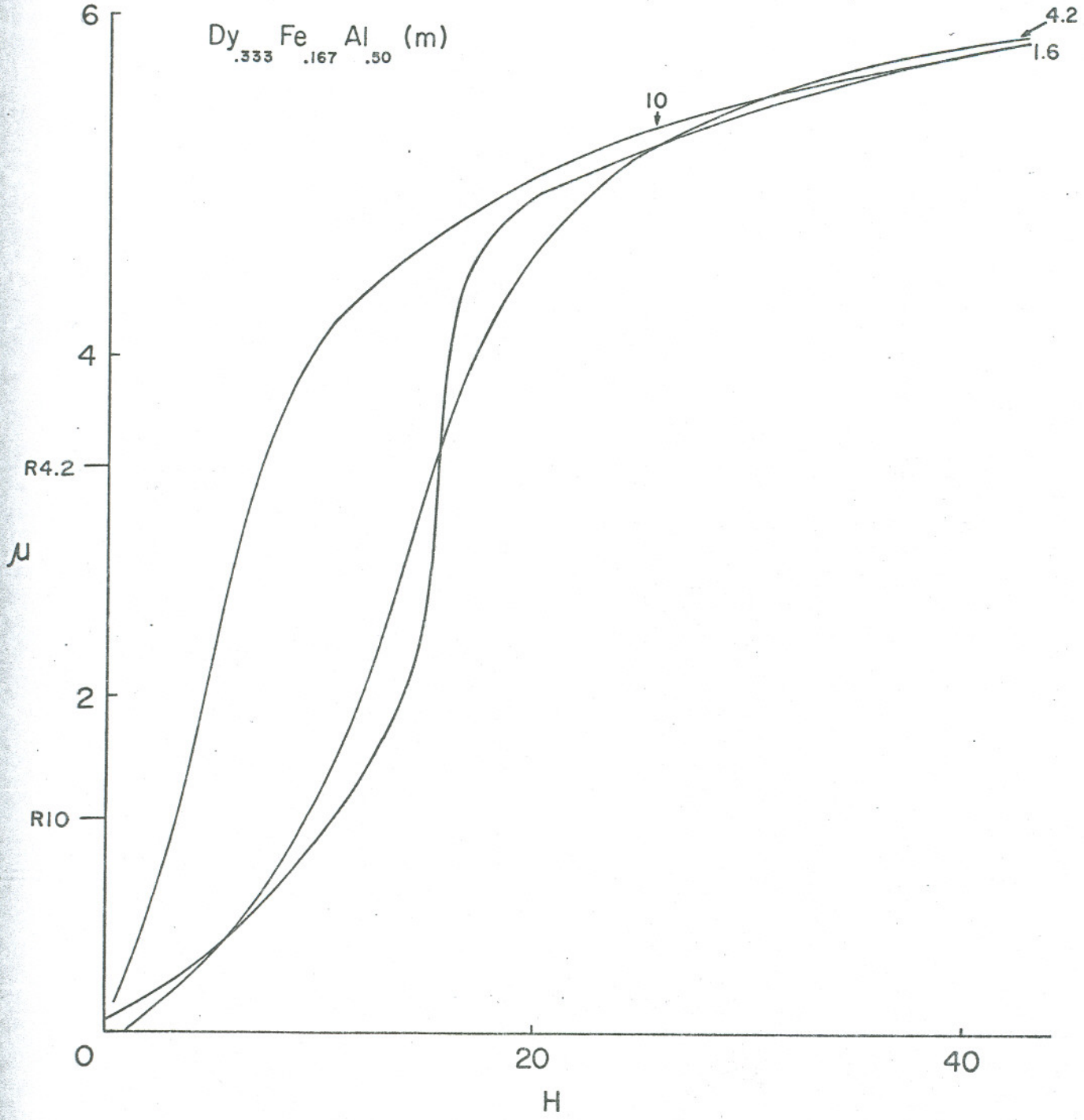

Fig 1 i

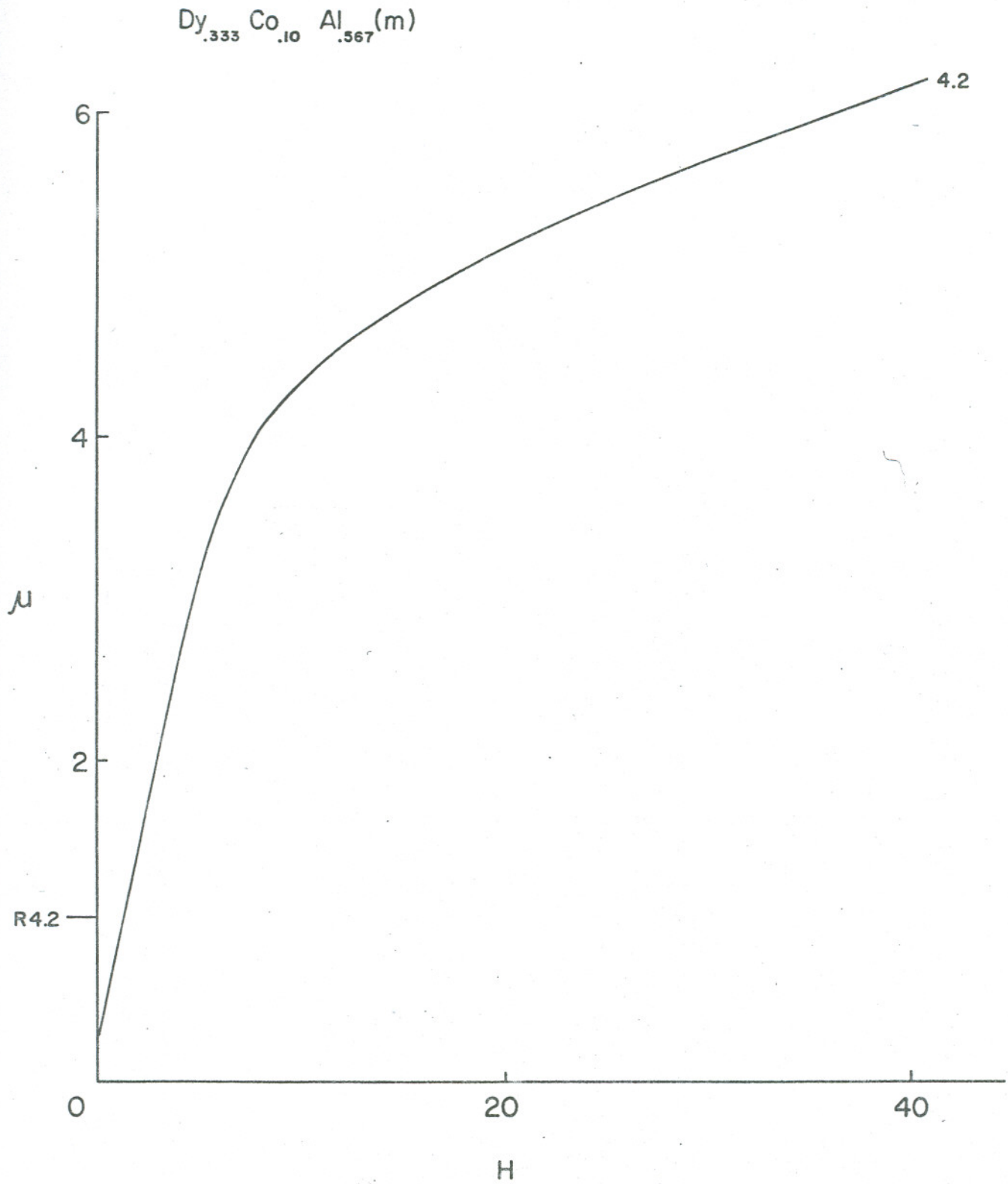

Fig 1 j

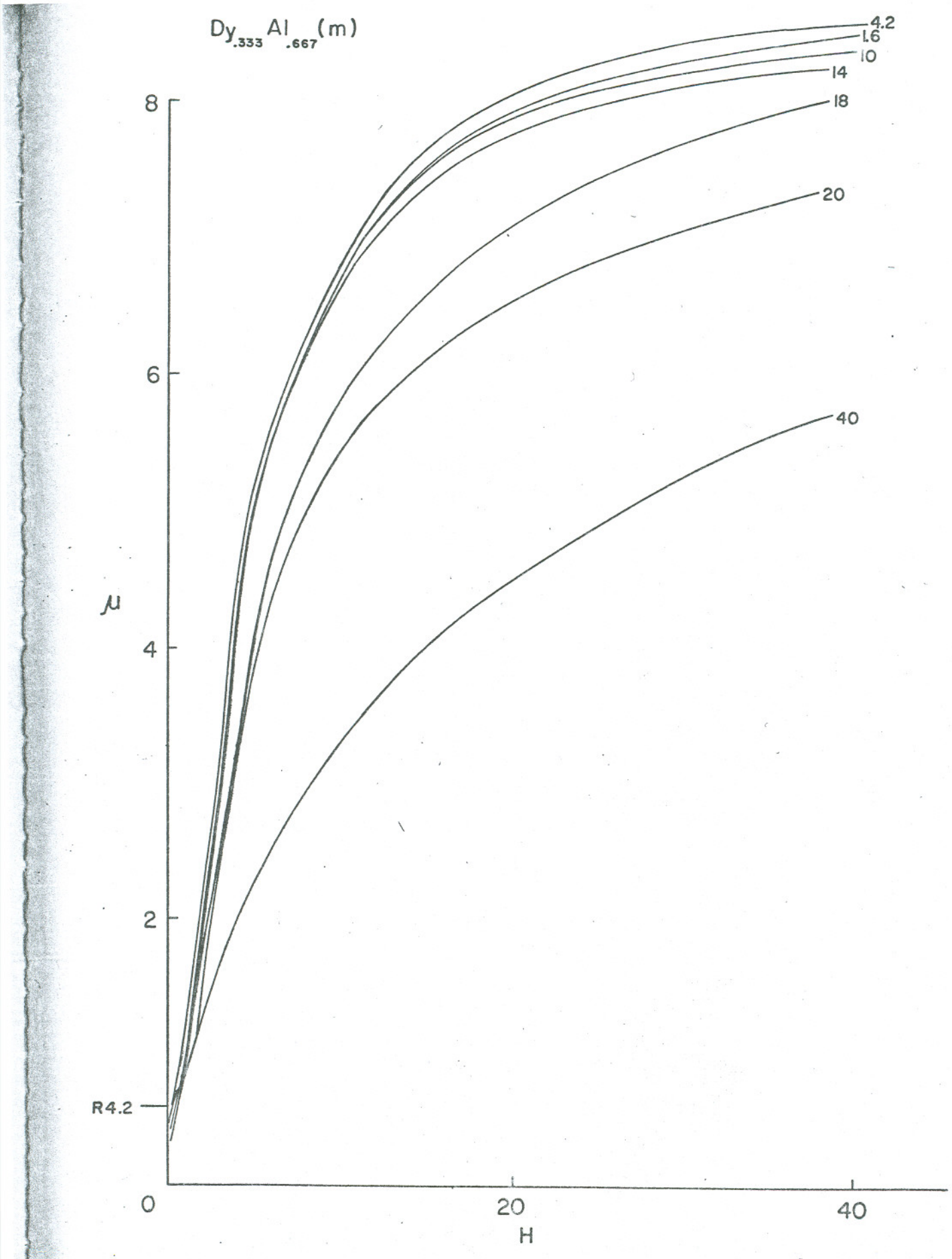

Fig 1-k

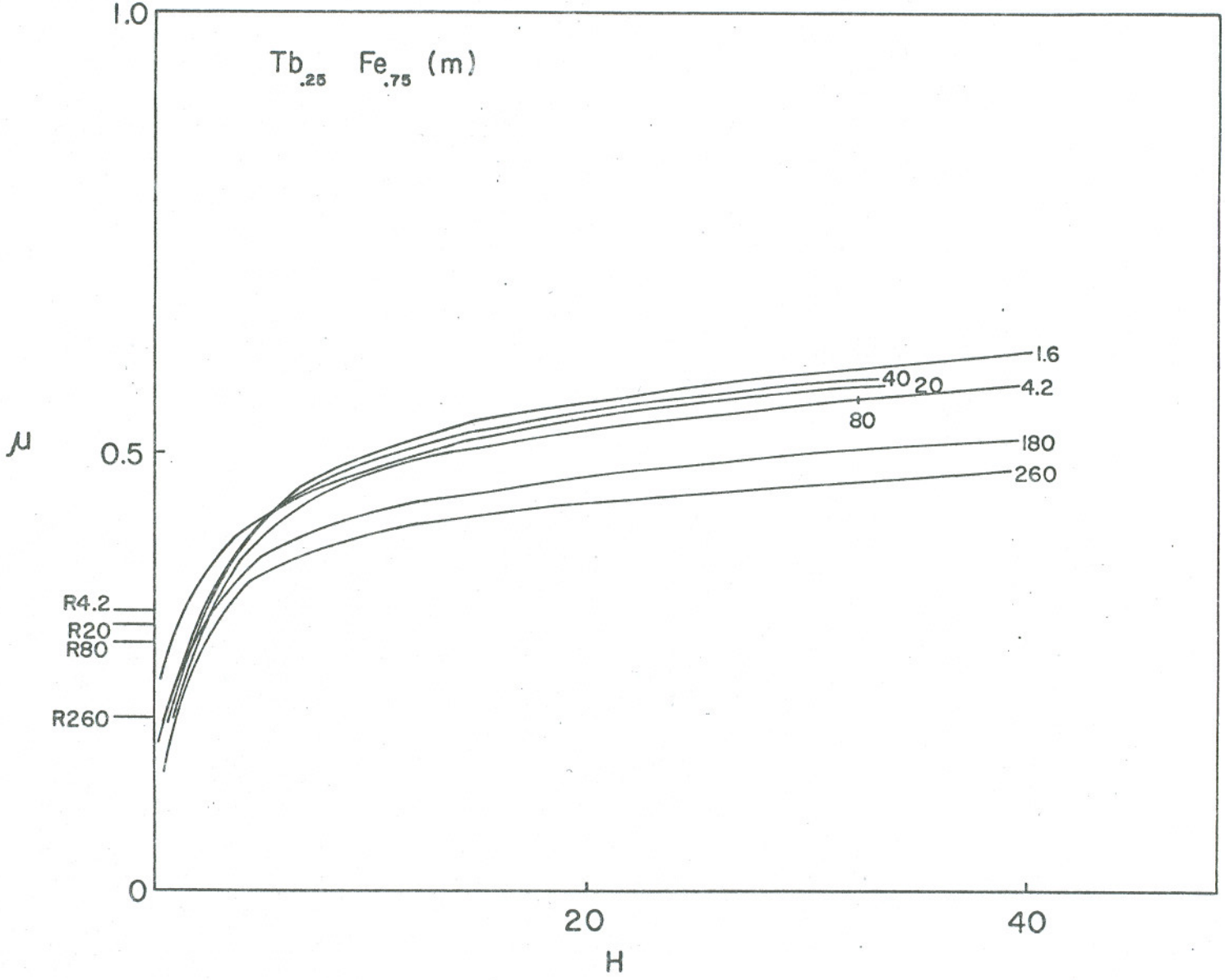

Fig 2a

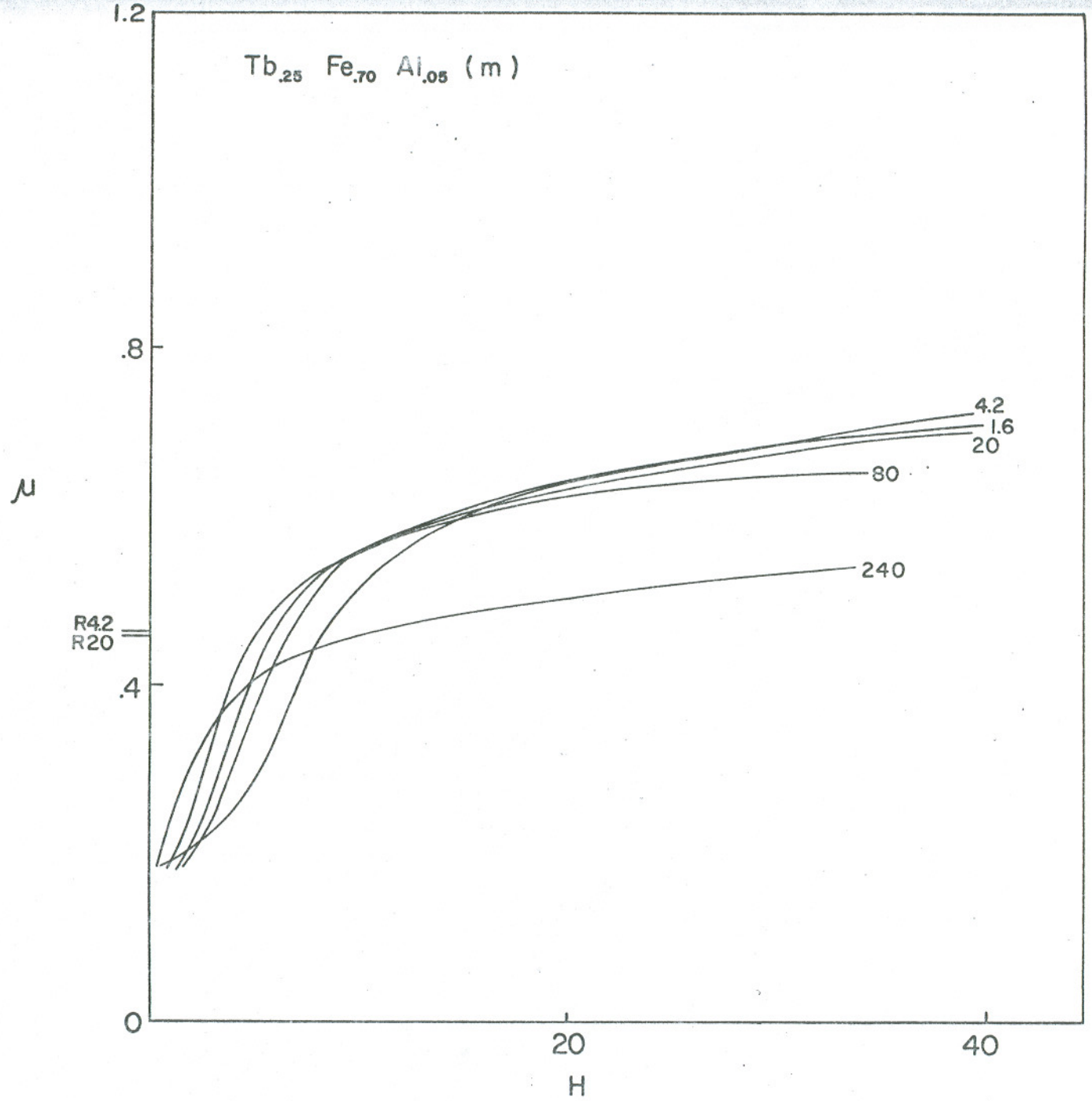

Fig 2b

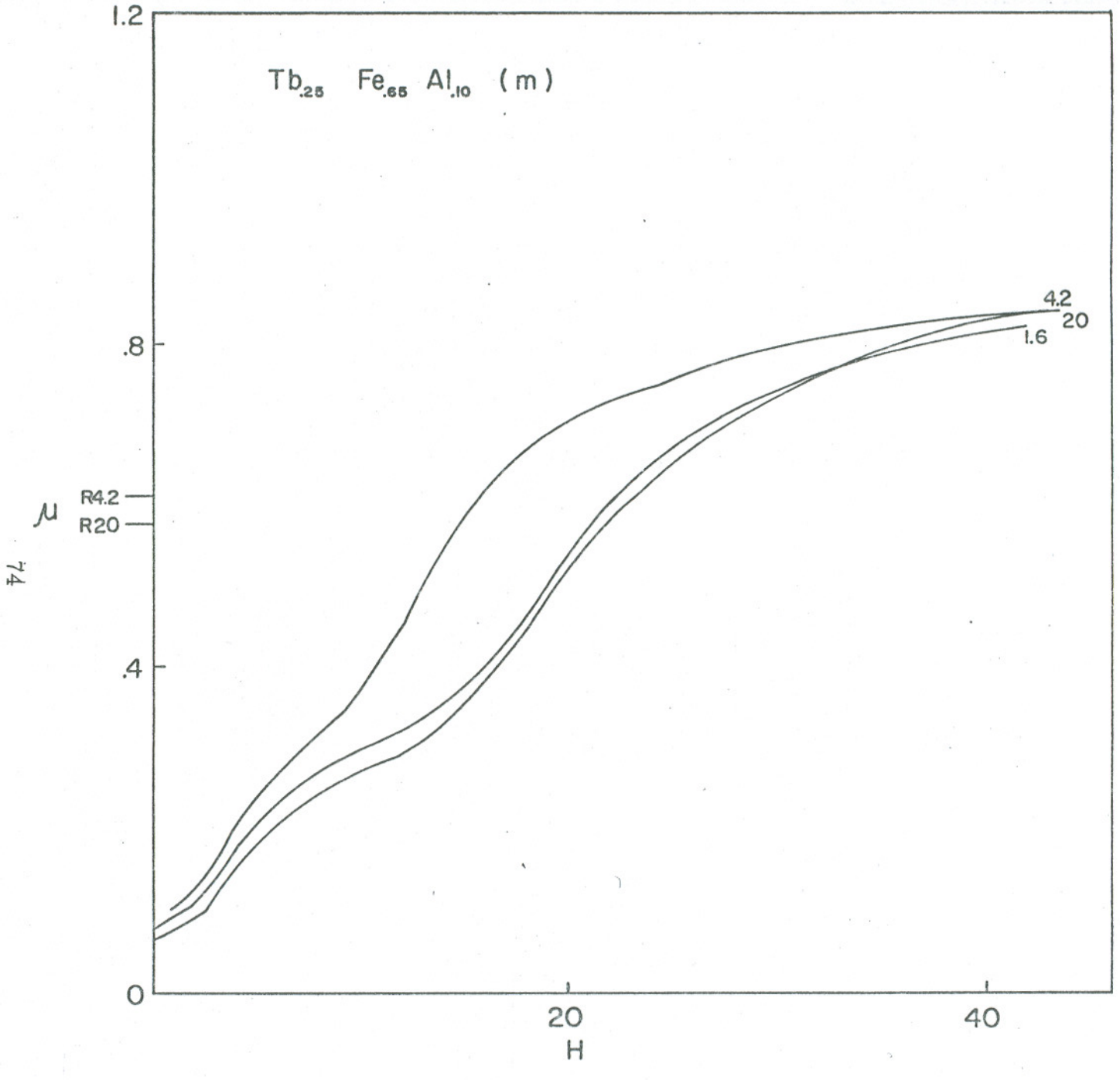

74

Fig 2c

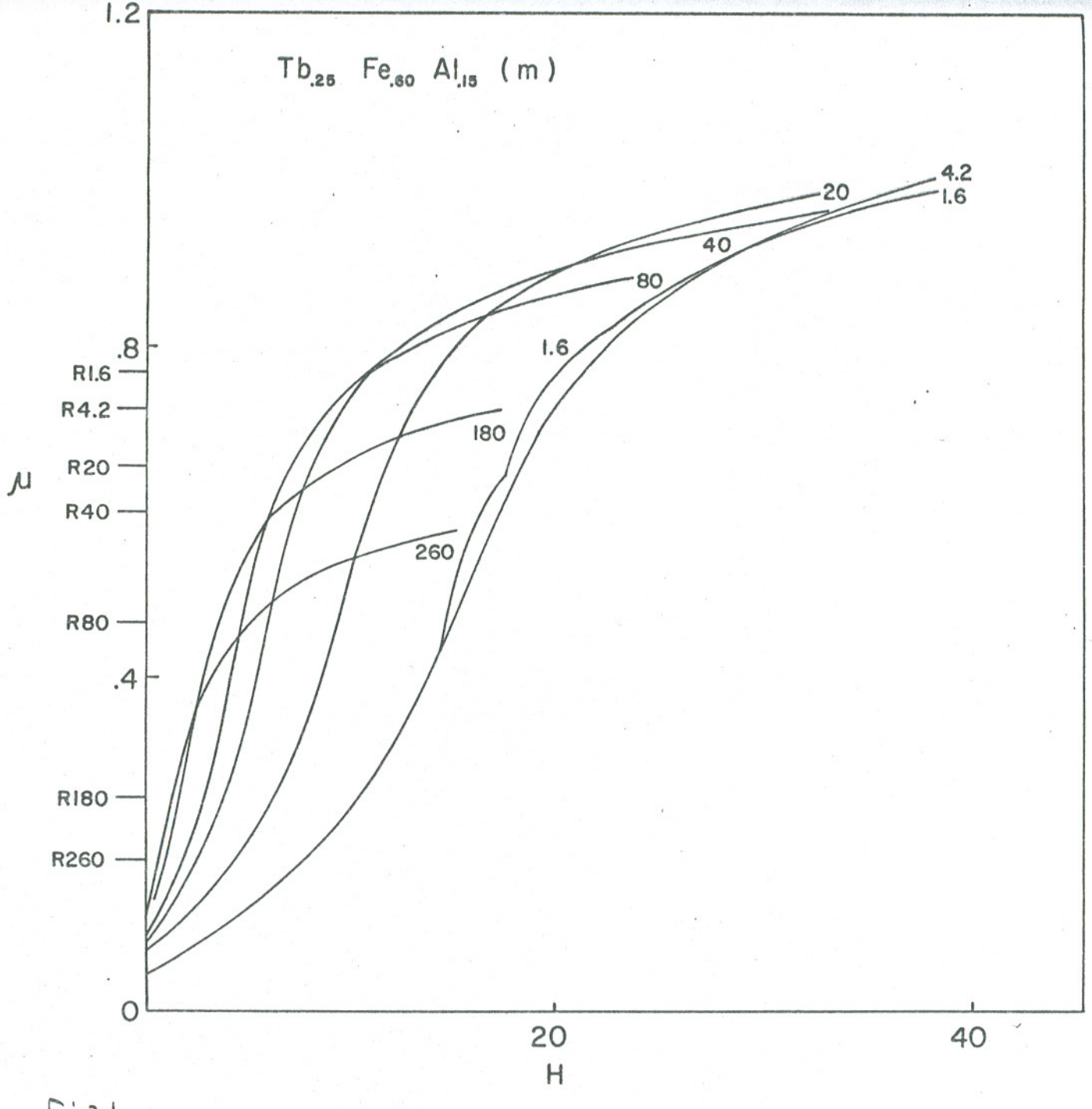
Tb.25 Fe.60 Al.15 (m)
1.2
.8
.4
0
μ
R1.6
R4.2
R20
R40
R80
R180
R260
4.2
1.6
20
40
80
180
260
1.6
20
40
H

Fig 2d

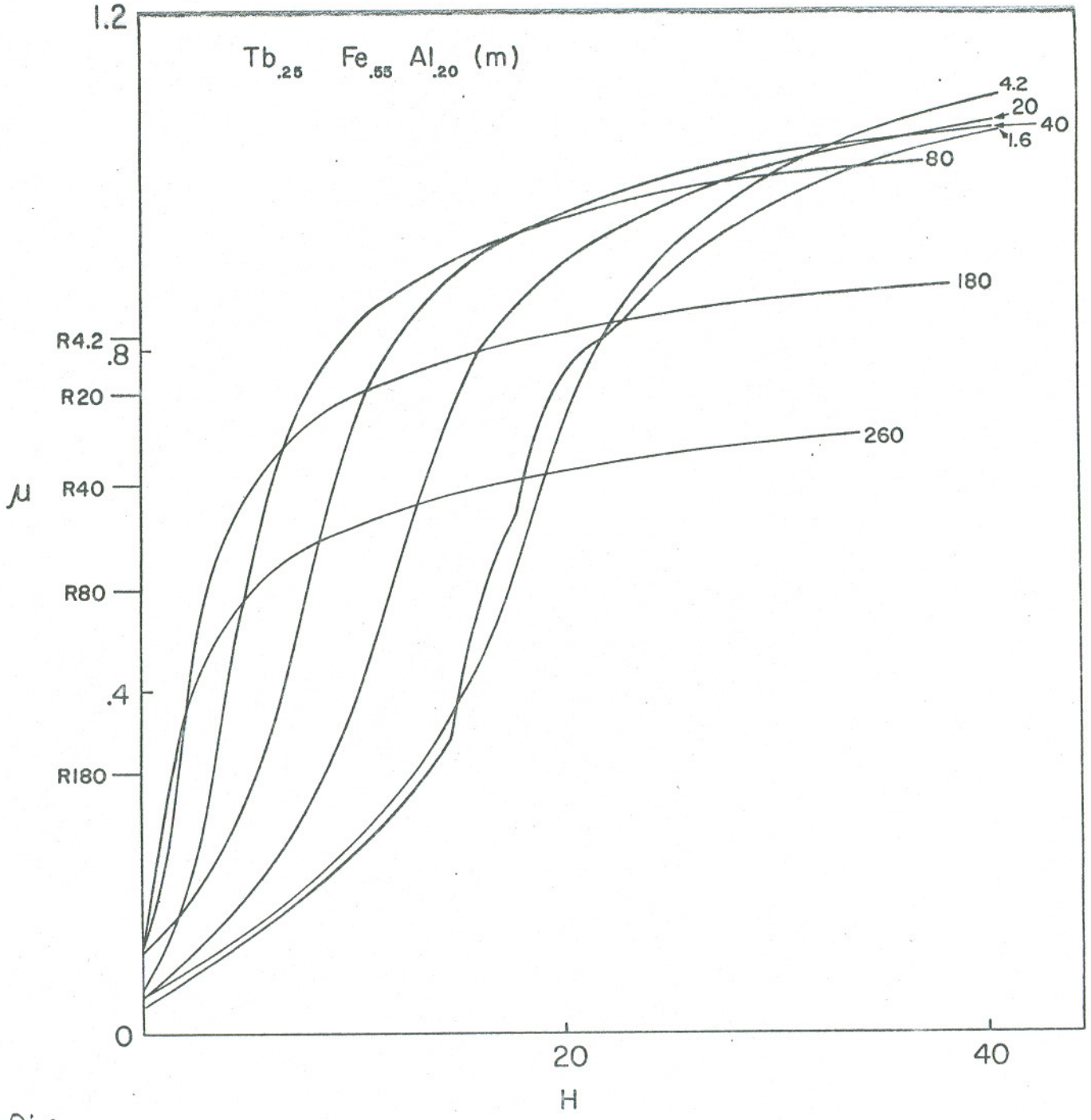
Tb.25 Fe.55 Al.20 (m)
1.2
.8
.4
0
μ
R4.2
R20
R40
R80
R180
4.2
20
40
1.6
80
180
260
20
40
H

fig 2e

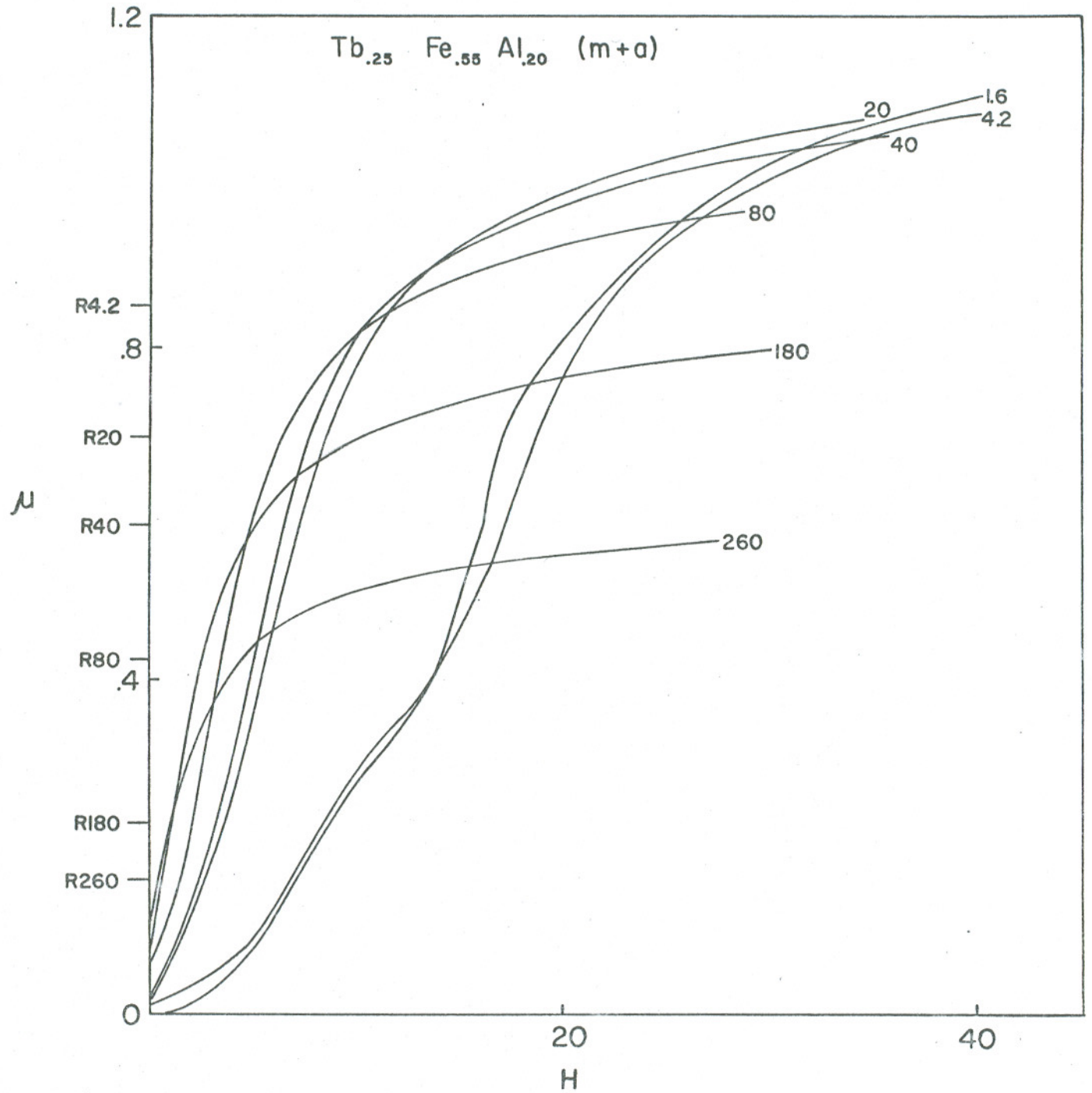
Tb.25 Fe.55 Al.20 (m+a)
1.2
.8
.4
0
μ
R4.2
R20
R40
R80
R180
R260
1.6
4.2
20
40
80
180
260
20
40
H

Fig 2

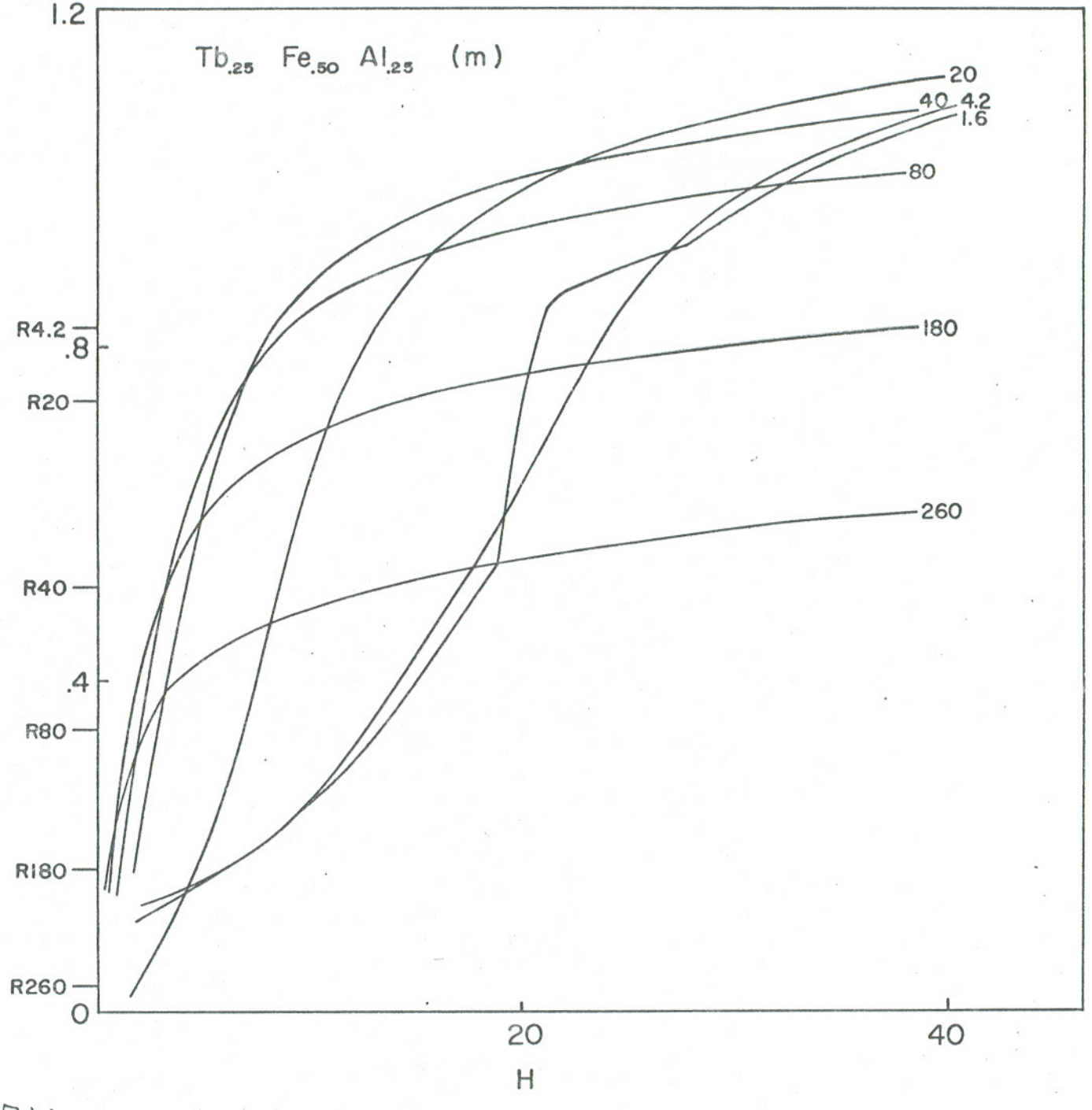
1.2
Tb.25 Fe.50 Al.25 (m)
20
40 4.2
1.6
80
180
260
R4.2
.8
R20
R40
.4
R80
R180
R260
0
20
40
H
μ

Fig 2g

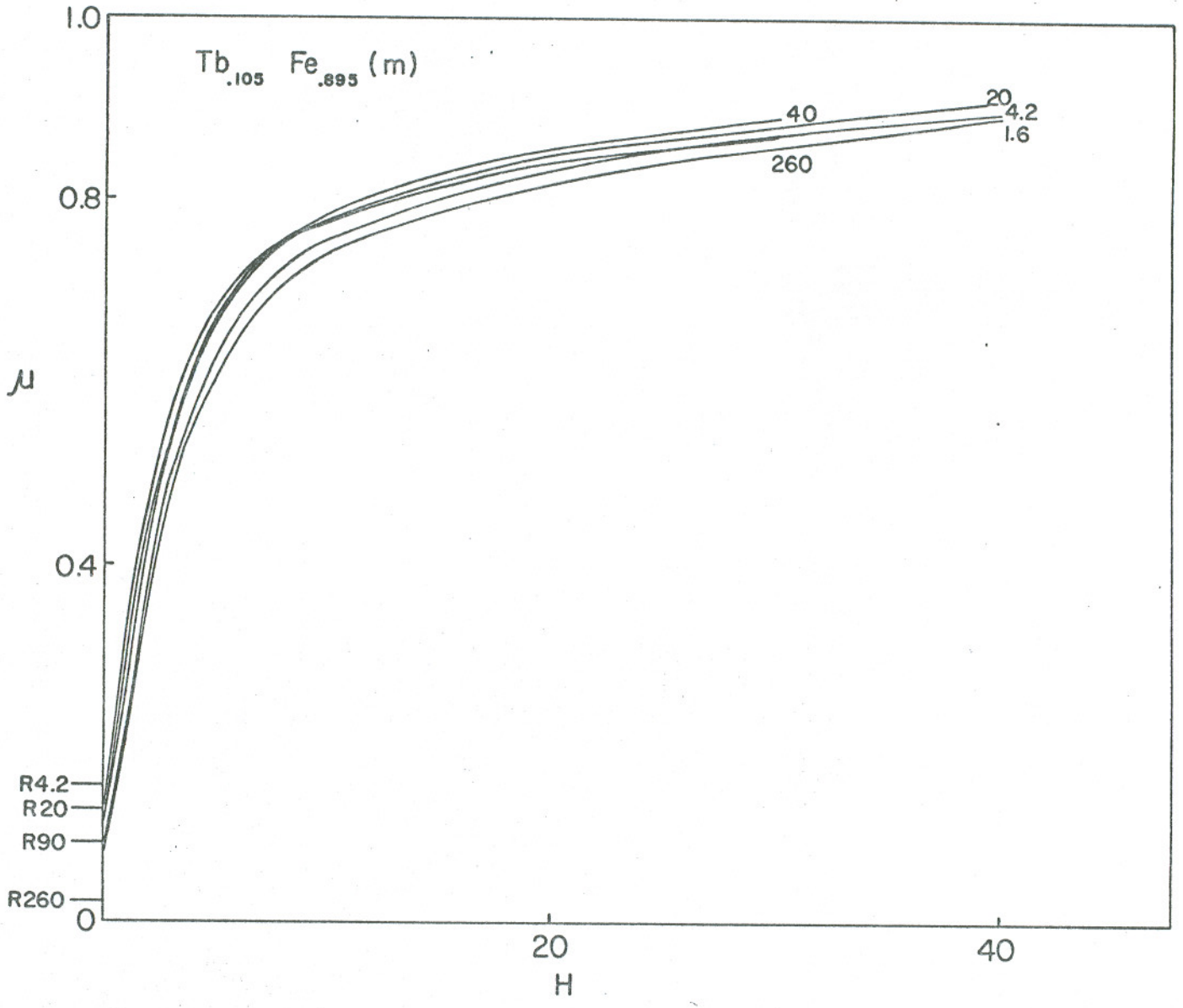

Fig 2 h

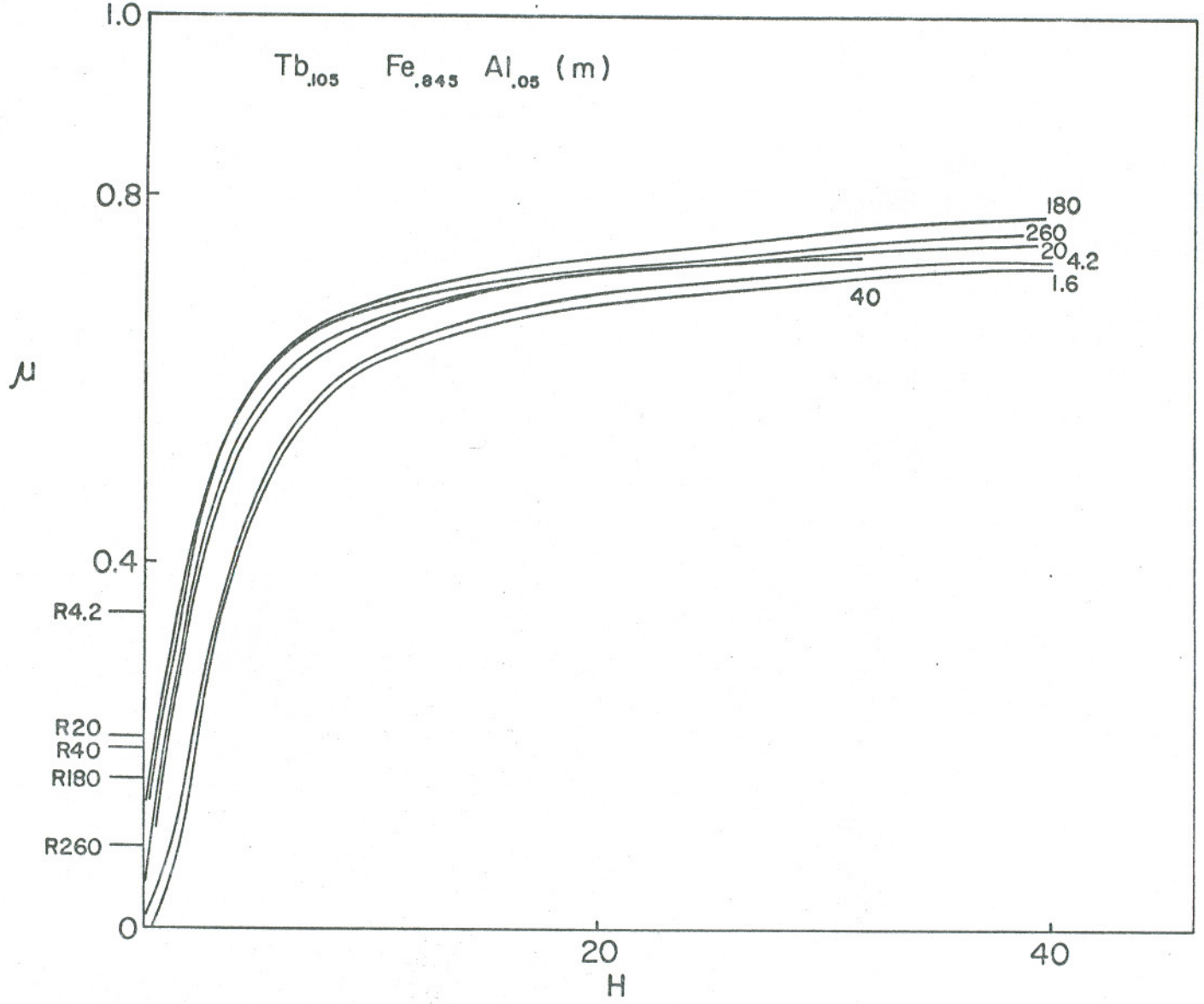
Tb.105 Fe.845 Al.05 (m)
1.0
0.8
0.4
0
μ
180
260
20
4.2
1.6
40
R4.2
R20
R40
R180
R260
20
40
H

Fig 2 i

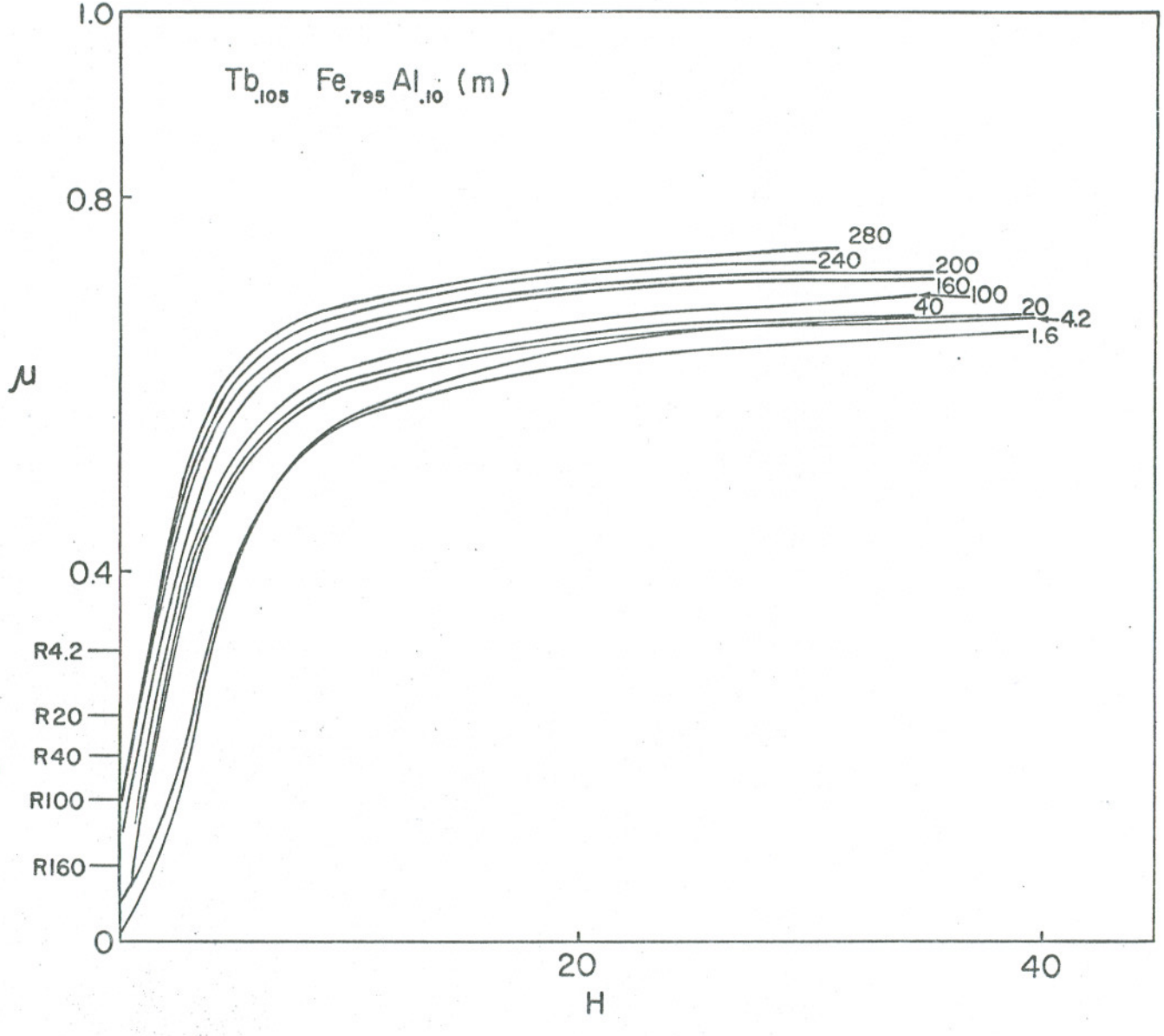
Tb.105 Fe.795 Al.10 (m)
1.0
0.8
0.4
0
μ
280
240
200
160
100
40
20
4.2
1.6
R4.2
R20
R40
R100
R160
20
40
H

Fig 2 j

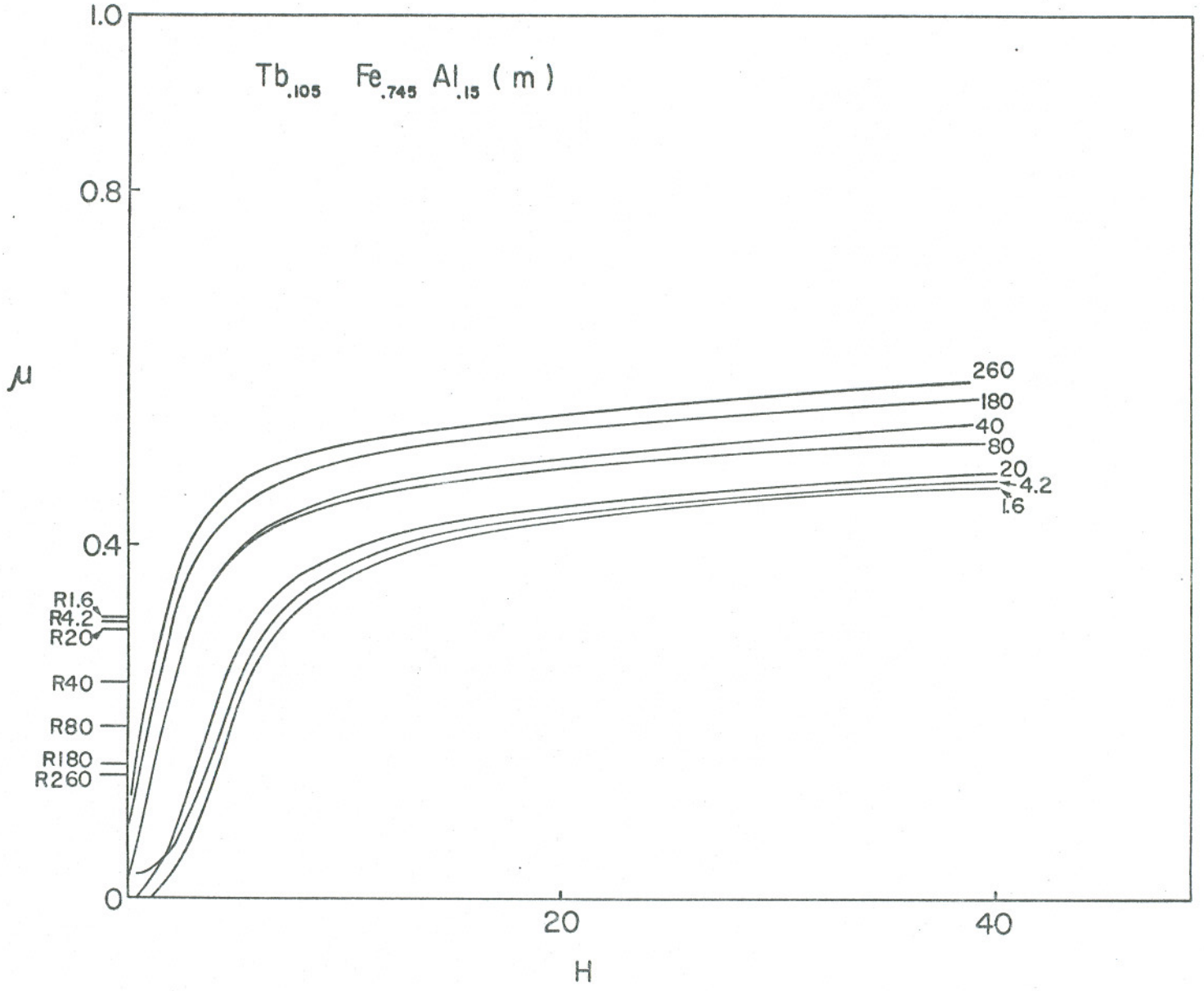
Tb.105 Fe.745 Al.15 (m)
1.0
0.8
0.4
0
μ
H
20
40
260
180
40
80
20
4.2
1.6
R1.6
R4.2
R20
R40
R80
R180
R260

Fig 2 k

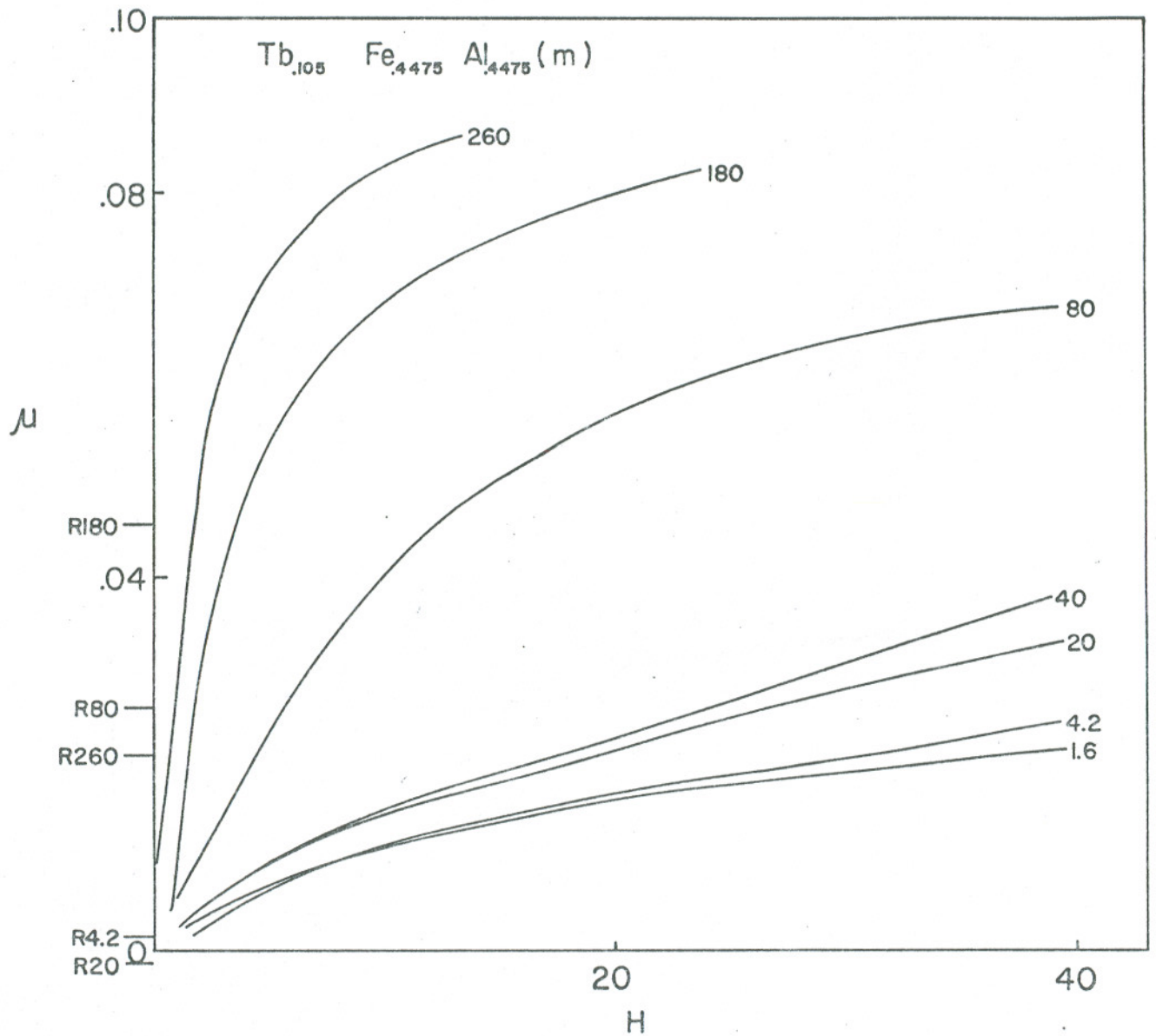
.10
.08
.04
Ω
μ
Tb.105 Fe.4475 Al.4475 (m)
260
180
80
40
20
4.2
1.6
R180
R80
R260
R4.2
R20
20
40
H

Fig 2 ℓ

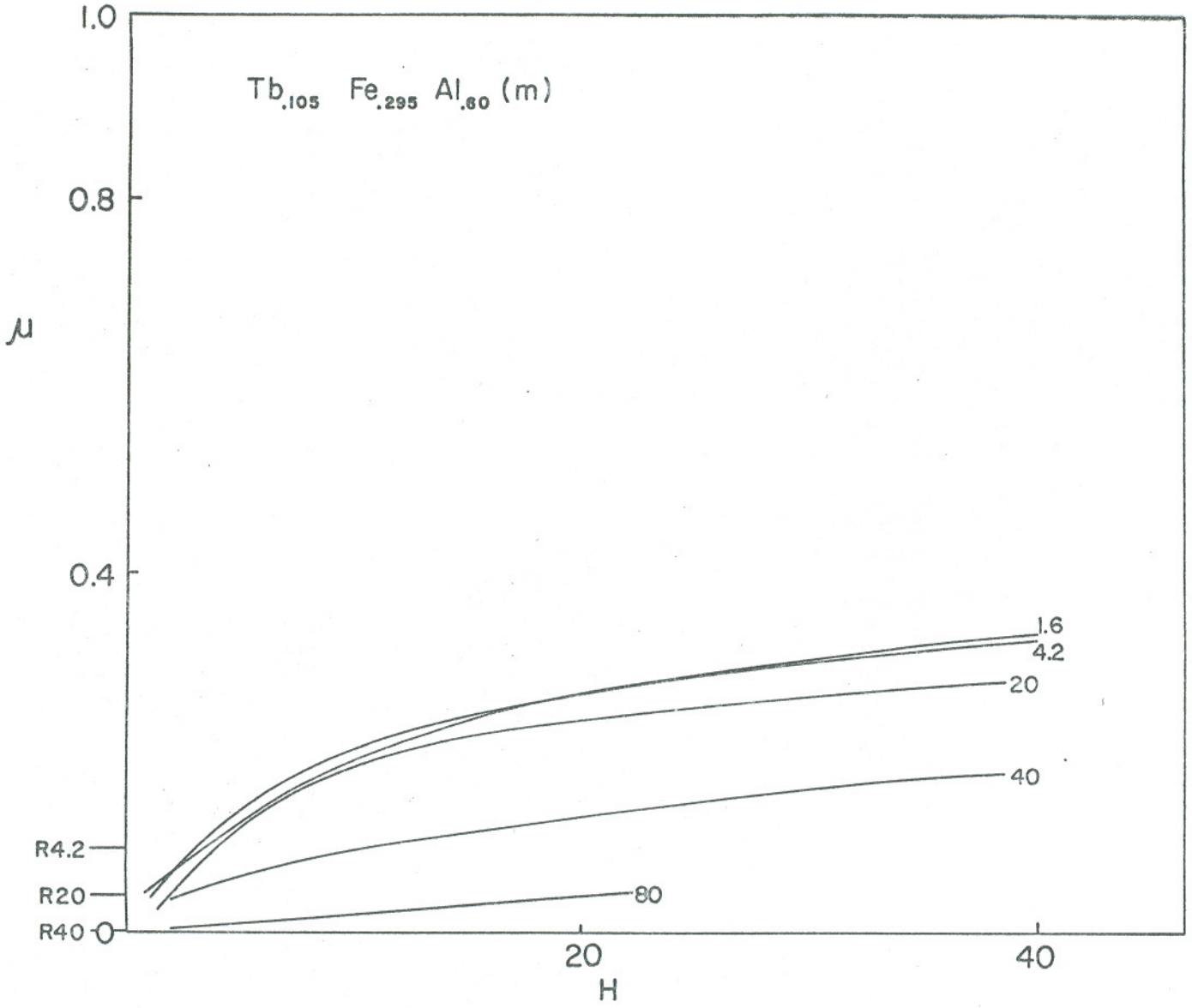

fig 2 m

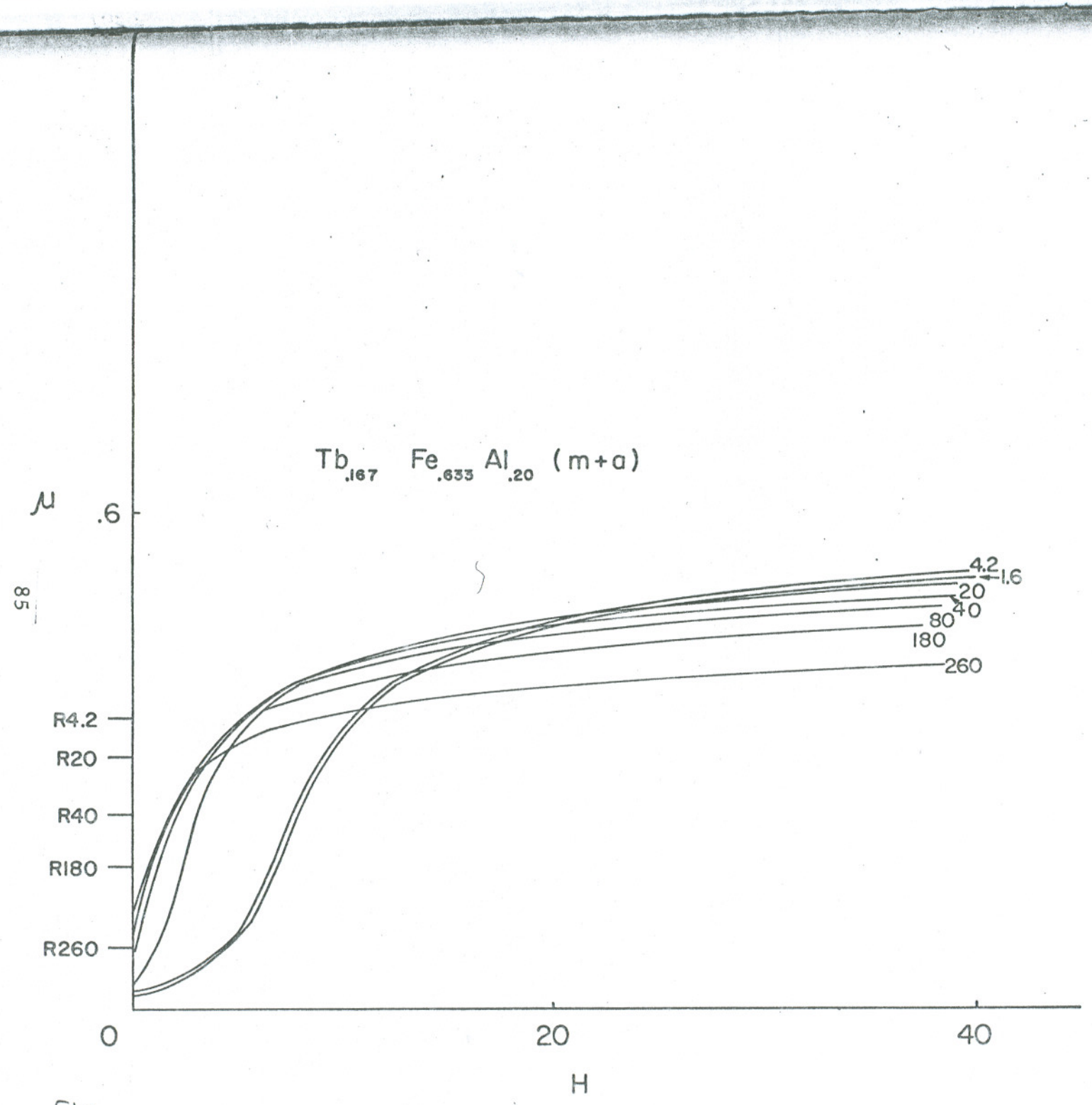
Tb.167 Fe.633 Al.20 (m+a)
μ
.6
85
4.2
1.6
20
40
80
180
260
R4.2
R20
R40
R180
R260
0
20
40
H

Fig 2 n

VII REFERENCES

1. M.V. Nevitt in P.A. Beck, Electronic Structure and Alloy Chemistry of Transition Elements, Wiley (1963).

2. R.P. Elliott and W. Rostocker, Trans. ASM, 50, 617 (1958).

3. A.E. Dwight, Trans. ASM, 53, 479 (1961).

4. H. Oesterreicher and W.E. Wallace, J. Less Comm. Metals, 13, 91 (1967).

5. K.H. T. Buschow, Phys. Stat. Solids (a) 7, 199 (1971).

6. D.T. Cromer and C.F. Olsen, Acta Cryst. 12, 689 (1959).

7. D.T. Cromer and A.C. Larson, Acta Cryst. 12, 855 (1959).

8. F.E. Wang, J.V. Gilfrich, D.H. Ernst and W.M. Hubbard, Acta. Cryst. 17, 931 (1964).

9. J.H. Wernick and S. Geller, Acta Cryst. 12, 662 (1959).

10. G. Bouchet, J. Laforest, R. Lemaire and J. Schweizer, C.R. Acad. Sc. Paris 262, 1227 (1966).

11. K.H.J. Buschow, J.Less-Comm. Metals, 16, 45 (1968).

12. J.H.N. van Vucht and K.H.J. Buschow, J. Less-Comm. Metals, 10, 98 (1965).

13. J. Farrell and W.E. Wallace, Inorg. Chem. 5, 105 (1966).

14. B. Bleany, Proc. Phys. Soc., 82, 469 (1963).

15. H.G. Purwins, Phys. Lett. 31A, 9, 523 (1970).

16. H.G. Purwins, Z. Phys. 233, 27 (1970).

17. G. Will, Z. Naturforsch, 23a, 413 (1968).

18. N. Nereson, C. Olson and G. Arnold, J. Appl. Phys.39,10,4605 (1968).

19. H. Oesterreicher, L.M. Corliss and J.M. Hastings, J.Appl.Phys., 41, 6, 2326 (1970).

20. W. Wiedemann and W. Zinn, Phys. Letters, 24A, 506 (1967).

21. H. Oesterreicher, J. de Physique, C1-1141 (1971).

22. H. Oesterreicher, J. Phys. Chem. Solids, 32, 1403 (1971).

23. B. Barbara, C. Becle, R. Lemaire and D. Paccard, J. de Physique, C1-299 (1971).

24. M.A. Rudermann and C. Kittle, Phys. Rev. 96, 99 (1954).

25. T. Kasuya, Progr. Theoret. Phys. 16, 45 (1956).

26. K. Yoshida, Phys. Rev. 106, 5 893 (1957).

27. D. Mattis and W.E. Donath, Phys. Rev. 128, 4, 1618 (1962).

28. A. J. Freeman and R.E. Watson, Phys. Rev. Letters, 14, 695 (1965).

29. K. Strnat, G. Hoffer, J. Olson and W. Ostertag and J.J. Becker, J. Appl. Phys., 38, 1001 (1967).

30. E. A. Nesbitt, J. Appl. Phys. 40, 1259 (1969).

31. J.J. Becker, Scientific American, 92 (1971).

32. E.A. Nesbitt, R.H. Willens, R.C. Sherwood, E. Buehler and J.H. Wernick, Appl. Phys. Letters, 12, 361 (1968).

33. J.H. Wernick, S.E. Hasks and D. Dorsi, J.Phys.Chem.Solids, 23, 567 (1962).

34. See. J.S. Kouvel, page 564 in Intermetallic Compounds by J.H. Westbrook, ed., John Wiley (1967).

35. K.H.J. Buschow and R.P. van Stapele, J. Phys. Suppl. 2-3, C1-672.

36. H. Oesterreicher, J. Less Comm. Metals, 25, 228 (1971).

37. H. Oesterreicher, J. Less Comm. Metals, 25, 341 (1971).

38. H. Oesterreicher, Solid State Comm. in print.

39. See C. Kittel, Introduction to Solid State Physics.

40. J.H. van Vucht and K.H.J. Buschow, J.Less Comm. Metals, 10, 98 (1965).

41. O.J.C. Runnalls and R.R. Boucher, J. Metals 15, 687 (1963).

42. K.H.J. Buschow and J.F. Fast, Zeitschr. Phys. Chem. 50, 1 (1966).

43. G.I. Hoffer and L.R. Salmans, Proc. 7th R.E. Res. Conf. 371 (1968).

44. K. Strnat, G.I. Hoffer and A.E. Ray, IEEE Trans. Magn. Mag.2, 489 (1966).

45. H. Oesterreicher, unpublished